ISTANBUL TECHNICAL UNIVERSITY ★ GRADUATE SCHOOL

DESIGN OF A HIGH-ACCURACY ENERGY MANAGEMENT SYSTEM FOR ELECTRIC VEHICLES AND V2G APPROACHES CONSIDERING BATTERY AGING

M.Sc. THESIS

Arda AKYILDIZ

Department of Electrical Engineering

Electrical Engineering Programme

AUGUST 2024

ISTANBUL TECHNICAL UNIVERSITY ★ GRADUATE SCHOOL

DESIGN OF A HIGH-ACCURACY ENERGY MANAGEMENT SYSTEM FOR ELECTRIC VEHICLES AND V2G APPROACHES CONSIDERING BATTERY AGING

M.Sc. THESIS

Arda AKYILDIZ
(504221003)

Department of Electrical Engineering

Electrical Engineering Programme

Thesis Advisor: Assoc. Prof. Dr. Mehmet Onur GÜLBAHÇE
Thesis Co-Advisor: Asst. Prof. Dr. Mustafa Alparslan ZEHİR

AUGUST 2024

ISTANBUL TEKNİK ÜNİVERSİTESİ ★ LİSANSÜSTÜ EĞİTİM ENSTİTÜSÜ

ELEKTRİKLİ ARAÇLAR İÇİN YÜKSEK DOĞRULUKLU ENERJİ YÖNETİM SİSTEMİ TASARIMI VE BATARYA YAŞLANMASINI DİKKATE ALAN V2G YAKLAŞIMLARI

YÜKSEK LİSANS TEZİ

Arda AKYILDIZ
(504221003)

Elektrik Mühendisliği Anabilim Dalı

Elektrik Mühendisliği Programı

Tez Danışmanı: Doç. Dr. Mehmet Onur GÜLBAHÇE
Eş Danışman: Dr. Öğr. Üyesi Mustafa Alparslan ZEHİR

AĞUSTOS 2024

Arda AKYILDIZ, a M.Sc student of ITU Graduate School student ID 504221003, successfully defended the thesis/dissertation entitled "DESIGN OF A HIGH ACCURACY ENERGY MANAGEMENT SYSTEM FOR ELECTRIC VEHICLES AND V2G APPROACHES CONSIDERING BATTERY AGING", which he prepared after fulfilling the requirements specified in the associated legislations, before the jury whose signatures are below.

Thesis Advisor :	**Assoc. Prof. Dr. Mehmet Onur GÜLBAHÇE** İstanbul Technical University	.....
Co-advisor:	**Asst. Prof. Dr. Mustafa Alparslan ZEHİR** Marmara University	.....
Jury Members :	**Prof. Dr. İlhan KOCAARSLAN** Istanbul Technical University	.....
	Asst. Prof. Dr. C. Fatih KÜÇÜKTEZCAN Istanbul Technical University	.....
	Dr. Ahmet Kubilay ATALAY ZS Kimya Elektronik San. Tic. A.Ş.	.....

Date of Submission : 22 July 2024
Date of Defense : 2 August 2024

To my dear family, for their endless support and the love they have shown,

FOREWORD

I would like to express my heartfelt gratitude to my family for their unwavering support and encouragement throughout this journey. Thanks to my friends for their companionship and understanding during challenging times. I am deeply thankful to Research Assistant Batı Eren Ergun for his invaluable guidance and collaboration. My sincere appreciation goes to Assoc. Prof. Dr. Mehmet Onur Gülbahçe and Assist. Prof. Dr. Mustafa Alparslan Zehir for their insightful advice and continuous support. Lastly, I extend my heartfelt thanks to Yaren for her constant motivation and inspiration. Without the support of these incredible individuals, this thesis would not have been possible.

This study was supported as part of the graduate thesis projects conducted by the Istanbul Technical University Scientific Research Projects Unit (Project No: MGA-2022-43948) and the Environmentally Compatible Sustainable Advanced Vehicle Technologies (İLATERA) (Project No: 22AG018). I would like to thank the Istanbul Technical University Scientific Research Projects Unit and TÜBİTAK for their support.

August 2024 Arda AKYILDIZ

TABLE OF CONTENTS

Page

ABBREVIATIONS

CEI : Cathode Electrolyte Interface

CO_2 : Carbon Dioxide

ECM : Equivalent Circuit Model

EV : Electric Vehicle

G2V : Grid-to-Vehicle

HF : Hydrofluoric Acid

LAM_{ne} : Loss of Active Material at the Negative Electrode

LAM_{pe} : Loss of Active Material at the Positive Electrode

LCO : Lithium Cobalt Oxide

LFP : Lithium Iron Phosphate

LLI : Lithium Inventory Loss

NCA : Nickel Cobalt Aluminum

NMC : Nickel Manganese Cobalt

RI : Resistance Increase

SEI : Solid Electrolyte Interphase

SOC : State of Charge

SOF : State of Function

SOH : State of Health

SOS : State of Safety

V2G : Vehicle-to-Grid

WLTP : Worldwide Harmonized Light Vehicles Test Procedure

SYMBOLS

A : Frontal Area of the Vehicle

A_h : Ampere-Hour Throughput

B : Pre-exponential Factor

C : Battery Capacity

C_0, C_1, C_2 : Rolling Resistance Coefficients

C_d : Aerodynamic Drag Coefficient

C_{rate} : Current Rate

DoD : Depth of Discharge

d : Gearbox Ratio

E_a : Activation Energy

E_b : Energy Output of the Battery

E_{tot} : Total Enregy

F_{aero} : Aerodynamic Drag Force

F_g : Gravitational Force

F_{res} : Forces Opposing the Vehicle's Motion

F_r : Wheel Rolling Resistance

I_{rate} : Current Rate

J_m : Motor Inertia

J_w : Wheel Inertia

N : Number of Cycles

P_{charge} : Charge Power

P_{air} : Atmospheris Pressure

P_{in} : Input Power

P_{out} : Output Power

P_{V2G} : Vehicle-to-Grid Charging/Discharcing power

P_{regen} : Regenerative Power

Q_{loss} : Capacity Loss

$Q_{loss, Calendar}$: Calendar Aging Loss

$Q_{loss, Cycle}$: Cycle Aging Loss

r : Wheel Radius

R **:** Gas Constant

R_{air} **:** Specific Gas Constant for Air

t : Time

T **:** Temperature

v **:** Speed

V **:** Volt

W **:** Wind Speed

β_1 **:** Pre-Exponential Fitting Factor

β_2 **:** Exponential Fitting Factor

-

LIST OF TABLES

Page

LIST OF FIGURES

Page

DESIGN OF A HIGH-ACCURACY ENERGY MANAGEMENT SYSTEM FOR ELECTRIC VEHICLES AND V2G APPROACHES CONSIDERING BATTERY AGING

SUMMARY

Smart grid technology uses digital communication technologies to optimize the processes of energy production, distribution, and consumption, providing more flexible, reliable, and efficient energy management compared to traditional energy production and distribution systems. This system has the capability to monitor and manage energy demand in real-time, allowing for more reliable use of energy resources and faster detection of faults in the grid.

The integration of renewable energy sources into smart grid systems is crucial for reducing the use of fossil fuels and meeting the increasing energy demand. When renewable sources such as solar, wind, hydroelectric, and geothermal energy are combined with smart grid technologies, they offer a sustainable and environmentally friendly approach to energy production and consumption. This integration increases energy efficiency while reducing the carbon footprint.

With the increasing use of electric vehicles, the necessity of vehicle-to-grid (V2G) service technology is also rising. V2G technology transforms the batteries of electric vehicles into energy sources that allow bidirectional energy flow. This integration enables electric vehicles to become not only consumers but also energy producers, providing feedback to the grid to balance energy demand fluctuations. Thus, the integration of renewable energy sources is facilitated, energy storage solutions become more effective, and grid stability is enhanced. The V2G integration of renewable energy systems plays a critical role, especially in ensuring the continuity of intermittent and irregular sources like solar and wind energy. By storing energy from these sources, electric vehicle batteries can supply energy to the grid when energy production is insufficient. This optimizes the balance of energy production and consumption, providing both economic and environmental benefits.

This study examines the frequency regulation service, one of the vehicle-to-grid services, in detail from the perspective of electric vehicle users. The study considers the battery aging and economic benefits of providing frequency regulation service when electric vehicles are connected to the grid.

First, to perform a realistic analysis, a comprehensive model was developed by considering various forces and factors affecting electric vehicles. In this model, factors such as traction forces, road characteristics, environmental forces, auxiliary systems, driving profile, and gravitational forces were examined. The traction forces of the electric vehicle are related to the torque produced by the motor and the power losses during the transmission of this torque to the wheels. Road characteristics are defined by parameters like road gradient, surface type, and friction coefficient. Environmental forces include external factors like air resistance and wind. Auxiliary systems consist of in-vehicle electronic systems, air conditioning, and other energy-consuming

components. The driving profile includes the vehicle's behaviors during acceleration, deceleration, stopping, and cruising. Gravitational forces determine the effect of the vehicle's weight on the road.

Then, battery aging mechanisms and factors affecting battery aging were examined in detail, and the Arrhenius battery aging model was used for lithium iron phosphate battery cells. The aging model was considered for two separate conditions: cycle aging due to regular use and charge-discharge cycles, and calendar aging occurring over time under storage or preservation conditions.

A battery pack was designed using four different lithium iron phosphate battery cells on the developed electric vehicle model. In this process, a selection algorithm was created by considering critical factors such as the volume, weight, cost, and aging of the battery pack. The algorithm aimed to make the most suitable selection by considering the different characteristics of each battery cell. For each battery cell, state of charge, state of health, and range data were analyzed. The state of charge indicates the current energy level of the battery, while the state of health evaluates the battery's lifespan and performance. Range data were examined to determine the distance the vehicle can travel on a single charge. Based on these analyses, the performance characteristics of each battery cell were compared, and the most suitable battery cell was selected. This comprehensive evaluation process aimed to offer an optimized solution for battery pack design in electric vehicles in terms of both performance and cost. Thus, the most suitable battery cell was selected for a long-lasting, cost-effective, and high-performance battery pack.

To plan vehicle-to-grid services, Great Britain's grid frequency data was used. One year of frequency data was clustered using the K-means clustering algorithm. The K-means clustering algorithm is a type of algorithm used to partition data from complex and large datasets into similar clusters. The algorithm was run multiple times iteratively to determine the days closest to the centroid of each cluster. In this way, the days that best represented each cluster were identified. The variances of the selected days were compared, and the 10 most different days exhibiting distinct characteristics were identified. These selected days were used to derive 10 years of grid frequency data, considering the percentage sizes of the clusters. The number of days in the 10-year dataset was distributed according to the percentage sizes of the clusters. The derivation process was carried out based on the available one-year frequency data to realistically reflect long-term scenarios.

Daily frequency data was divided into 30-minute periods, and optimization was performed with a binary genetic algorithm by assigning various weights in terms of revenue and battery aging of the electric vehicle. The binary genetic algorithm is a method where decision variables are represented in binary form and are evolutionarily optimized through genetic operators. This algorithm is population-based, with each individual evaluated as a solution proposal. New generations are formed using operators such as selection, crossover, and mutation, evolving towards the best solution.

The scenario considers that the electric vehicle goes on a trip twice a day, once at 9:00 AM and once at 6:00 PM, each lasting 30 minutes. During each trip, the vehicle travels a total of 23 kilometers. The vehicle is charged every day between 11:00 PM and 11:59 PM and starts each day with an 80% state of charge. For the remaining time, the vehicle is assumed to be available for V2G frequency regulation service. The V2G service can operate bidirectionally when the state of charge is between 90% and 40%. If the state

of charge is above 90%, the battery can only be discharged through the V2G service. If the state of charge falls below 40%, the battery can only be charged through the V2G service. The optimization algorithm decides whether to provide vehicle-to-grid service during different periods of the day according to various weights. During this process, an optimal strategy is developed in line with grid demands and the vehicle owner's income expectations. The study examines a total of six different scenarios. These scenarios compare the effects of different charging station powers, such as 11 kW and 3.7 kW, on revenue and battery aging. For each charging power, optimal results are obtained under conditions of minimizing battery aging, maximizing revenue, and 50% revenue, 50% battery aging weights.

In conclusion, while the 11 kW charging station provides more revenue in the V2G service, the battery aging rate is also higher. This situation is related to the higher stress caused by the high charging power on the battery, which shortens the battery life in the long term. On the other hand, while 3.7 kW nominal power stations provide less revenue, the battery aging rate is also lower.

.

ELEKTRİKLİ ARAÇLAR İÇİN YÜKSEK DOĞRULUKLU ENERJİ YÖNETİM SİSTEMİ TASARIMI VE BATARYA YAŞLANMASINI DİKKATE ALAN V2G YAKLAŞIMLARI

ÖZET

Akıllı şebeke teknolojisi, geleneksel enerji üretim ve dağıtım sistemlerinden daha esnek, güvenilir ve verimli bir enerji yönetimi sağlamak amacıyla dijital iletişim teknolojilerini kullanarak enerji üretimi, dağıtımı ve tüketimi süreçlerini optimize eder. Bu sistem, enerji talebini gerçek zamanlı olarak izleyip yönetme yeteneğine sahiptir ve enerji kaynaklarının daha güvenilir kullanılmasına, şebekede oluşabilecek arızaların daha hızlı tespit edilmesine olanak tanır.

Yenilenebilir enerji kaynaklarının akıllı şebeke sistemlerine entegrasyonu, fosil yakıt kullanımını azaltma ve artan enerji talebini karşılama hedefleri doğrultusunda büyük önem taşır. Güneş, rüzgar, hidroelektrik ve jeotermal enerji gibi yenilenebilir kaynakları akıllı şebeke teknolojileri ile birleştirildiğinde enerji üretimi ve tüketiminde sürdürülebilir ve çevre dostu bir yaklaşım sunar. Bu entegrasyon, enerji verimliliğini artırırken karbon ayak izini de azaltır.

Günden güne artan elektrikli araç kullanımı ile birlikte araçtan şebekeye hizmet teknolojisine olan ihtiyaç artmaktadır. V2G teknolojisi elektrikli araçların bataryalarını çift yönlü enerji akışına imkan tanıyan birer enerji kaynağına dönüştürür. Bu entegrasyon sayesinde elektrikli araçlar yalnızca tüketici değil, aynı zamanda enerji üreticisi haline gelir ve şebekeye geri besleme yaparak enerji talep dalgalanmalarını dengeleyebilir. Böylece yenilenebilir enerji kaynaklarının entegrasyonu kolaylaşır, enerji depolama çözümleri daha etkin hale gelir ve şebeke kararlılığı arttırılmış olur. Yenilenebilir enerji sistemlerinin V2G entegrasyonu, özellikle güneş ve rüzgar enerjisi gibi kesintili ve düzensiz kaynakların sürekliliğini sağlamada kritik bir rol oynar. Elektrikli araç bataryaları, bu tür kaynaklardan elde edilen enerjiyi depolayarak, enerji arzının yetersiz olduğu zamanlarda şebekeye enerji sağlar. Bu durum, enerji üretim ve tüketim dengesini optimize ederek hem ekonomik hem de çevresel faydalar sağlar.

Bu çalışmada elektrikli araç kullanıcısı perspektifinden bakılarak V2G hizmetlerinden biri olan frekans regülasyonu detaylı bir şekilde incelenmiştir. Çalışma kapsamında elektrikli araçların şebekeye bağlanarak frekans regülasyonu hizmeti sağlama süreci, batarya yaşlanması ve ekonomik getirileri açısından değerlendirilmiştir.

İlk olarak, gerçekçi bir analiz gerçekleştirmek amacıyla, elektrikli araçlar üzerinde etkili olan çeşitli kuvvetler ve etkenler dikkate alınarak kapsamlı bir model geliştirilmiştir. Bu modelde temel kuvvetler, çekiş kuvvetleri, yol karakteristiği, çevresel kuvvetler, yardımcı sistemler, sürüş profili ve yerçekimsel kuvvetler gibi faktörler incelenmiştir. Elektrikli aracın çekiş kuvvetleri, motorun ürettiği moment ve bu momentin tekerleklere iletilmesi sırasında oluşan güç kayıplarıyla ilişkilidir. Yol karakteristiği ise yolun eğimi, yüzey tipi ve sürtünme katsayısı gibi parametrelerle tanımlanır. Çevresel kuvvetler, hava direnci ve rüzgar gibi dış etkenleri kapsar. Yardımcı sistemler, araç içi elektronik sistemler, klima, ve diğer enerji tüketen

bileşenlerden oluşur. Sürüş profili ise aracın hızlanma, yavaşlama, durma ve seyir halindeki davranışlarını içerir. Yerçekimsel kuvvetler ise aracın ağırlığının yol üzerindeki etkisini belirler.

Batarya yaşlanma mekanizmaları ve batarya yaşlanmasına etki eden faktörler detaylı bir şekilde incelenmiş ve bu incelemeler kapsamında lityum demir fosfat batarya hücreleri için Arrhenius batarya yaşlanma modeli kullanılmıştır. Yaşlanma modelini iki ayrı durum için ele alınmıştır. İlki bataryanın düzenli kullanımı sırasında meydana gelen ve şarj-deşarj döngüleri sonucunda meydana gelen çevrim yaşlanması, diğeri ise bataryanın depolama veya muhafaza koşullarında zamanla meydana gelen takvim yaşlanmasıdır.

Geliştirilen elektrikli araç modeli üzerinde dört farklı lityum demir fosfat batarya hücresi kullanılarak batarya paketi tasarlanmıştır. Bu süreçte batarya paketinin hacmi, ağırlığı, maliyeti ve batarya yaşlanması gibi kritik faktörler dikkate alınarak bir seçim algoritması oluşturulmuştur. Algoritmanın oluşturulmasında her bir batarya hücresinin farklı özellikleri göz önünde bulundurularak en uygun seçimin yapılması hedeflenmiştir. Her bir batarya hücresi için ayrı ayrı şarj durumu, sağlık durumu ve menzil verileri analiz edilmiştir. Şarj durumu, bataryanın mevcut enerji seviyesini belirtirken sağlık durumu bataryanın kullanım ömrü ve performansını değerlendirmekte kullanılmıştır. Menzil verileri ise aracın tek bir şarjla kat edebileceği mesafeyi belirlemek amacıyla incelenmiştir. Bu analizler sonucunda her bir batarya hücresinin performans özellikleri karşılaştırılmış ve elde edilen veriler doğrultusunda en uygun batarya hücresinin seçimi yapılmıştır. Bu kapsamlı değerlendirme sürecinde elektrikli araçların batarya paketi tasarımı hem performans hem de maliyet açısından optimize edilmiştir. Böylece uzun ömürlü, maliyet etkin ve yüksek performanslı bir batarya paketi için en uygun batarya hücresi seçilmiştir.

Araçtan şebekeye hizmet planlaması yapmak amacıyla Büyük Britanya şebeke frekans verileri kullanılmıştır. Elde edilen 1 yıllık frekans verileri, K-means sınıflandırma algoritması kullanılarak kümeleme işlemi yapılmıştır. K-means sınıflandırma algoritması, karmaşık ve büyük veri setlerine ait verileri birbirine benzer kümelere ayırmakta kullanılan bir algoritma türüdür. K-means algoritması, iterasyonlar boyunca birçok kez çalıştırılarak her bir kümenin ağırlık merkezine en yakın günler belirlenmiştir. Bu şekilde, her kümenin en iyi temsilcisi olan günler tespit edilmiştir. Seçilen günlerin birbirlerine göre varyansları karşılaştırılmış ve bu analiz sonucunda, birbirlerinden farklı karakteristik özellikler sergileyen en farklı on gün tespit edilmiştir. Bu seçilen günler, kümelerin yüzdesel büyüklükleri göz önünde bulundurularak, on yıllık şebeke frekans verisi türetilmesinde kullanılmıştır. Kümelerin yüzdesel büyüklüklerine göre on yıllık veri setinde de gün sayıları, aynı yüzdesel büyüklüklere göre dağıtılmıştır. Türetme işlemi, elde bulunan bir yıllık frekans verisinden yola çıkarak gerçekleştirilmiş olup, bu sayede uzun dönemli senaryoların daha gerçekçi bir şekilde yansıtılması amaçlanmıştır.

Günlük frekans verileri otuz dakikalık periyotlara bölünerek elektrikli aracın gelir ve batarya yaşlanması açısından çeşitli ağırlıklar verilerek ikili genetik algoritma ile optimizasyonu yapılmıştır. İkili genetik algoritma, karar değişkenlerinin ikili biçimde temsil edildiği ve bu değişkenlerin genetik operatörler aracılığıyla evrimsel olarak optimize edildiği bir yöntemdir. Bu algoritma, popülasyon tabanlı olup, her birey bir çözüm önerisi olarak değerlendirilir. Seçim, çaprazlama ve mutasyon gibi operatörler kullanılarak yeni nesiller oluşturulur ve en iyi çözüme doğru evrimleşme sağlanır.

Senaryo olarak elektrikli araç, her gün iki kere sürüşe çıkmaktadır. Bu sürüşlerden biri sabah 09:00'da, diğeri ise akşam 18:00'de gerçekleşmektedir ve her biri otuz dakika sürmektedir. Her bir sürüş sırasında araç toplamda yirmi üç kilometre yol kat etmektedir. Araç her gün gece 23:00 ile 23:59 saatleri arasında şarj edilmektedir ve her güne %80'lik bir şarj durumu ile başlamaktadır. Geri kalan süre boyunca ise aracın, V2G frekans regülasyonu hizmeti sunmaya müsait olduğu varsayılmaktadır. V2G hizmeti, aracın şarj durumu %90 ile %40 arasında olduğunda çift yönlü olarak çalışabilmektedir. Eğer şarj durumu %90'ın üzerinde ise, batarya yalnızca V2G hizmeti aracılığıyla deşarj olabilmektedir. Şarj durumu %40'ın altına düştüğünde ise batarya yalnızca V2G hizmeti ile şarj olabilmektedir. Optimizasyon algoritması çeşitli ağırlıklara göre günün farklı periyotlarında araçtan şebekeye hizmetin yapılıp yapılmayacağına karar vermektedir. Bu süreçte, şebeke taleplerine ve araç sahibinin gelir beklentilerine uygun optimal bir strateji geliştirilir. Çalışmada, toplamda altı farklı senaryo incelenmiştir. Bu senaryolar arasında 11 kW ve 3.7 kW olmak üzere farklı şarj istasyonu güçlerinin gelir ve batarya yaşlanması üzerine etkileri karşılaştırmalı bir şekilde ele alınmıştır. Her bir şarj gücü için batarya yaşlanmasını minimize eden, geliri maksimize eden ve %50 gelir, %50 batarya yaşlanması ağırlıkları altında en uygun sonuçlar elde edilmiştir.

Sonuç olarak, 11 kW gücündeki şarj istasyonu, V2G hizmetinde daha fazla gelir sağlarken, bataryanın yaşlanma hızı da daha yüksek olmuştur. Bu durum, yüksek şarj gücünün batarya üzerinde daha fazla stres yaratarak uzun vadede batarya ömrünü kısaltmasıyla ilişkilendirilmiştir. Öte yandan, 3.7 kW nominal gücündeki istasyonlar daha düşük gelir sağlamakla birlikte, batarya yaşlanma hızı da daha düşük olmuştur.

1. INTRODUCTION

The use of fossil fuels causes the release of large amounts of harmful gases such as carbon dioxide (CO_2) into the atmosphere, leading to the greenhouse effect and global warming. This situation results in air pollution, acid rain, rising sea levels, and a decrease in biodiversity. Due to such effects, it is necessary to make changes in global energy policies for more environmentally friendly solutions. In this context, turning to renewable energy sources, reducing the use of fossil fuels, and developing sustainable energy solutions are important both environmentally and economically.

Renewable energy plants, by their nature, cannot continuously and regularly produce energy. Solar power plants operate efficiently during daylight hours and on sunny days, while wind power plants operate efficiently when wind speeds are sufficient. This irregularity causes energy fluctuations in the electrical grid, reducing grid stability and decreasing energy quality. Energy storage systems help the grid by minimizing these demand and supply imbalances, meeting instantaneous energy demands, and enabling the continuous use of renewable energy sources. By storing excess energy produced during the day or windy times, they save it to be used during periods of high energy demand or reduced production. This situation increases energy efficiency and facilitates the integration of renewable energy.

With advancing technology and innovative solutions, interest in Electric Vehicles (EVs) is increasing day by day. Compared to internal combustion engine vehicles, they have many advantages. These include:

- Energy Efficiency: EVs are much more efficient in energy conversion compared to internal combustion engines. With regenerative braking technology, they recover some of the energy consumed during braking to recharge the battery. Thus, overall energy efficiency is increased, and the range is extended.
- Environmentally Friendly: Electric vehicles operate with zero gas emissions. This improves air quality in cities and reduces greenhouse gas emissions. As

the number of EVs charged with renewable energy sources increases, the carbon footprint is further reduced.

- Low Operating Costs: Electricity is cheaper than gasoline and diesel. This provides cost savings for users in daily use.
- Performance: Electric motors provide instant maximum torque, offering higher acceleration. Additionally, placing the battery pack at the base of the vehicle provides a low center of gravity. This increases road handling, reduces the likelihood of rollover, and improves driving safety.
- Compatibility with Renewable Energy Systems: Electric vehicles can work compatibly with renewable energy sources such as solar and wind. Thanks to advanced battery technologies and smart charging systems, electric vehicles can operate integrated with the grid. By charging during times of low electricity demand, they help balance the load on the grid.

Considering these factors, electric vehicles offer a more environmentally friendly and sustainable transportation option.

Another important point is the batteries used in electric vehicles. The lifespan of batteries used in electric vehicles is one of the main components in terms of vehicle performance and cost. Depending on usage conditions and duration, there are decreases in battery capacity. As a result of battery aging, various performance losses occur compared to the vehicle's initial usage. Typically, li-ion batteries complete their lifespan after 500 – 3000 charge-discharge cycles [1] . With advancing technology, efforts are being made to extend battery life through both battery technology and energy management systems that take battery aging into account along with battery management systems. After completing their first life, these batteries have various applications in their second life. Although these batteries no longer operate at full capacity, they can be used in fixed systems or to provide services to the electrical grid in conjunction with renewable energy production such as wind and solar power [2].

Vehicle-to-Grid (V2G) technology is a system that allows electric vehicles (EVs) to feed the energy stored in their batteries back into the electric grid. This technology is based on the principle of using bidirectional chargers, enabling electric vehicles to both store energy and return it to the grid when needed. The Schematic diagram of V2G technology is shown in Figure 1.1.

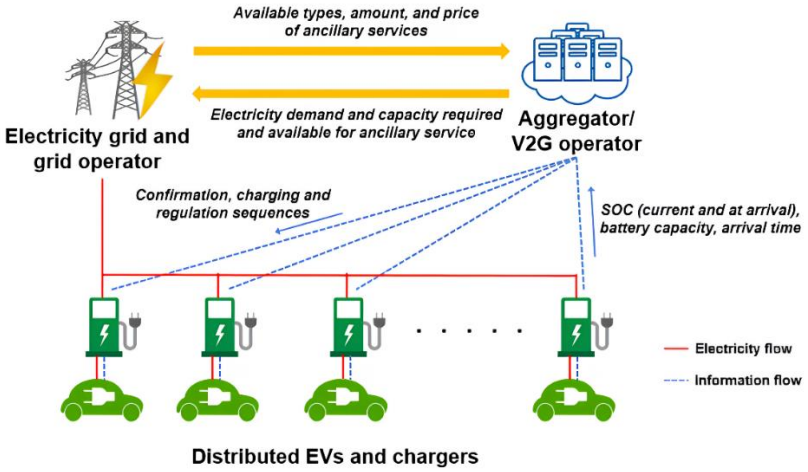

Figure 1.1 : Schematic diagram of V2G technology [3].

V2G technology offers significant advantages in energy demand management. Electric grids typically require backup energy sources to meet increases in energy demand (peak loads). V2G technology helps balance energy demand by using the energy stored in electric vehicle batteries to meet these peak loads. This allows the grid to operate more efficiently and reduces energy costs. It also supports grid stability through services such as voltage and frequency regulation [4].

The widespread adoption of V2G technology will be accelerated by the development of charging infrastructure and the establishment of standards. The reduction in the cost and increase in the efficiency of bidirectional chargers will enable V2G technology to reach a broader user base. Additionally, governments and energy regulatory bodies should develop regulations and support programs that promote V2G technology. This will encourage both consumers and energy providers to invest in V2G systems [5].

1.1 Purpose of Thesis

This study discusses the integration of electric vehicles into grid services, with a detailed focus on vehicle-to-grid technology from the user perspective. The potential benefits and challenges of V2G technology, as well as the interactions between electric vehicles and the grid, are examined. Based on real-world data, a comprehensive analysis of battery aging and the economic benefits of V2G frequency regulation service over a ten-year usage period of an electric vehicle is conducted. During the analyses, a genetic algorithm-based optimization method is used for frequency regulation service planning, employing a cost function that considers 50% battery

aging and 50% revenues. Additionally, strategies to reduce battery aging and increase revenue are planned and the results are compared. The study also examines 11 kW and 3.7 kW charging stations, comparing the results of these two different charging stations under the same cost constraints. The comparisons reveal specific advantages and disadvantages of each charging station, and optimal strategies for electric vehicle drivers are developed based on these findings.of the V2G frequency regulation service, both economically and in terms of battery aging, were emphasized and optimal strategies were developed for electric vehicle drivers.

1.2 Literature Review

The examination of battery chemistries used in electric vehicles is critically important for the performance and efficiency of the vehicles. When analyzing the battery chemistries used, it is generally observed that lead-acid, nickel-based, sodium-sulfur, and lithium-ion batteries are utilized [6]. However, the majority of batteries preferred in today's electric vehicles are lithium-ion batteries. Compared to other battery types, lithium-ion batteries are more favored in the market due to their high power energy density, low maintenance cost, long life cycle, and high efficiency [6-9].

In batteries, performance is largely determined by the cathode chemistry. While graphite is generally preferred in the anode section of lithium-ion batteries, the use of different lithium compounds in the cathode section significantly affects the performance of these batteries [6-9].

Nickel Cobalt Aluminum (NCA) and Nickel Manganese Cobalt (NMC) battery types exhibit largely similar characteristics in terms of performance. Both types provide high power and energy, as well as a long life cycle. The source of high energy in these battery chemistries is the amount of nickel; therefore, nickel-rich batteries with reduced cobalt content will also have high energy density [9]. Additionally, studies indicate that future cobalt reserves will be depleted, so it is anticipated that the amount of cobalt used in batteries will be reduced [8,10]. Lithium Cobalt Oxide (LCO) batteries are less preferred compared to other batteries due to their limited cobalt content and short life cycle. Lithium Iron Phosphate (LFP) battery type is preferred for its long life cycle and high electrochemical performance, and it operates over a wide temperature range. Figure 1.2 shows a comparative illustration of different battery chemistries.

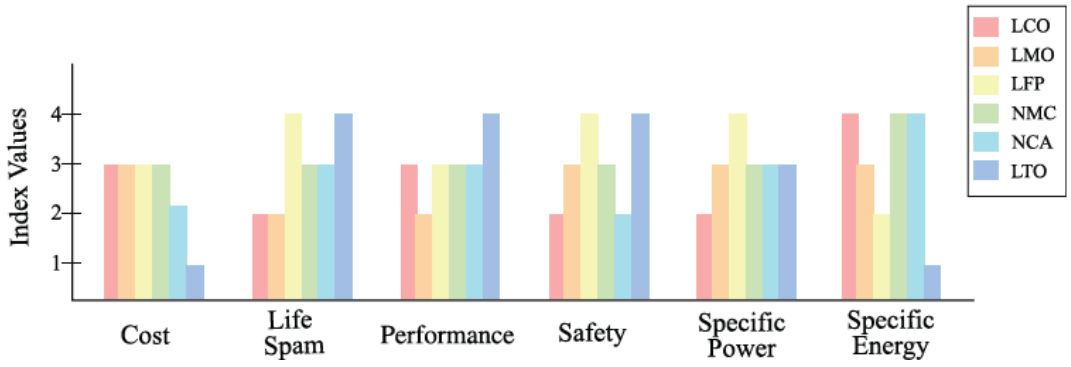

Figure 1.2 : Comparison of battery cells under various criteria [6].

In recent years, battery manufacturers have been shifting towards nickel-rich and cobalt-reduced battery chemistries (such as NMC811, NMC955) for low-cost and higher energy batteries. In 2020, the demand for cobalt decreased from 24% to 18%, and the increasing prices due to diminishing cobalt reserves have also driven this trend. On the other hand, for heavy-duty and medium-sized vehicles, manufacturers prefer low-cost LFP batteries that do not require high energy density. Due to high raw material prices, LFP batteries are becoming increasingly attractive [10].

According to a scenario in the report published by the International Energy Agency, the use of LFP batteries is expected to increase by 2030, and the majority of NMC batteries will consist of high-nickel batteries. In another scenario in the report, it is predicted that LFP batteries will dominate the market in the event of a continued increase in metal prices [10]. Figure 1.3 shows the estimated usage rate by battery chemistry over the years.

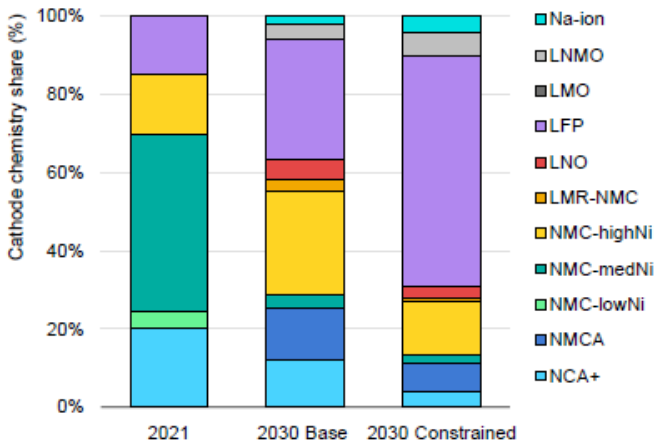

Figure 1.3 : Estimated usage distribution by battery chemistry from 2021 to 2030 [10].

There are numerous studies in the literature on V2G technology. These studies comprehensively address the impacts and potential benefits of V2G from both the grid and user perspectives. From the grid perspective, V2G technology provides flexibility in energy storage and management, offering advantages such as load balancing and emergency backup. From the user perspective, economic incentives and sustainability benefits stand out.

[11] introduces a V2G operation that aims to reduce ownership costs and contribute to grid services by optimizing the charging/discharging of electric vehicles. The proposed system supports voltage and frequency regulation by optimizing energy forecasting with day-ahead planning and real-time data. Simulations conducted on the IEEE 33-node distribution network with five EV charging stations demonstrate the potential to meet active and reactive power demands during peak periods while reducing EV charging costs.

Alfaverrh et al. (2024) state that the expanding Electric Vehicle market makes it possible for EVs to deliver a variety of grid services. Vehicle-to-Grid technology with a bi-directional power grid provides mobile energy storage to the grid for services such as demand regulation and frequency regulation. This can be profitable for customers, grid operators and energy supplies while reducing cost-intensive electricity costs. The study specifies an optimal V2G control strategy with Deep Reinforcement Learning to simultaneously maximize the benefits of EV owners and foragers by offsetting the reproductive costs of EV owners. The strategy performs frequency regulation operations by dynamically adjusting V2G power planning with the Deep Deterministic Policy Gradient agent. A two-area power economy tested proposal was implemented more effectively than other strategies by reducing frequency drift and improving Area Control Error [12].

In [13], V2G models are proposed to integrate EVs into power systems. The main objectives include reducing peak demand, decreasing the variance of the load profile, minimizing battery degradation costs, and lowering EV charging/discharging costs based on real-time pricing. The study considers EV driving patterns, including distance, duration, and charging/discharging levels and locations. A nonlinear battery degradation cost function is linearized and incorporated into the models. Additionally, a distributed control algorithm is developed to implement the optimal models. One-day simulation results show that the proposed approach reduces peak demand by 7.8%

and load profile variance by 81.9%, significantly improving power system stability and energy efficiency. Furthermore, the combined EV charging/discharging cost and battery degradation cost decrease from $251 to -$153, indicating that 100 EVs can earn $153 in a day through the V2G program.

1.3 Hypothesis

With the development of smart grid technology, vehicle-to-grid services are expected to become widespread. With this expansion, an optimum management system will be required that takes into account users' income and battery aging, while also increasing the stability and reducing of the grid load. The hypothesis of this thesis is to evaluate V2G service in terms of battery aging and revenue for electric vehicle users. The optimization algorithm developed based on real-world data supports the claims made by this hypothesis.

2. ELECTRIC VEHICLE MODEL

For vehicle energy consumption estimation, fundamental forces acting on the vehicle, tractive forces, ambient forces, gravitational forces, temperature, humidity and air density, road type (city, highway, etc.), traffic situation, driving style (aggressive driving, eco driving, etc.), auxiliary systems (headlights, air conditioning, etc.) and the route to be taken are important for realistic predictions. These factors were shown in Figure 2.1.

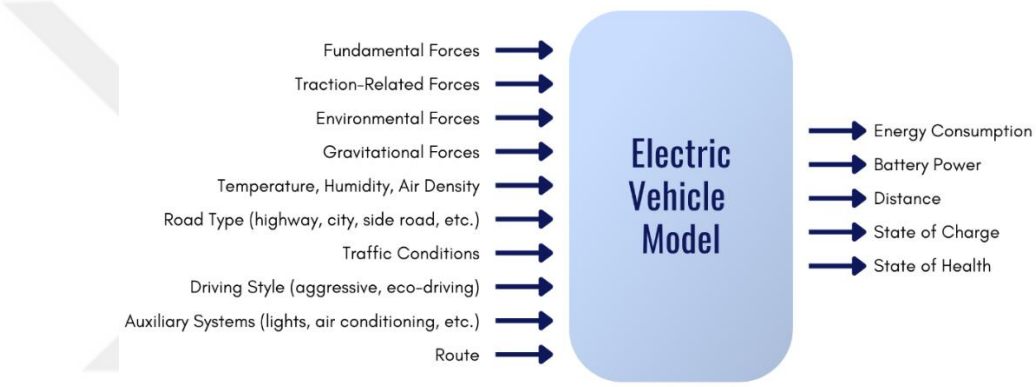

Figure 2.1 : Factors considered in the electric vehicle model.

2.1 Acting Forces on the Vehicle

The forces acting on the vehicle are wheel rolling resistance, aerodynamic drag force of the vehicle, gravitational force and acceleration forces. The net force can be expressed as the sum of these forces as in equation 2.1 [14]. The acting forces on the vehicle are shown in Figure 2.2.

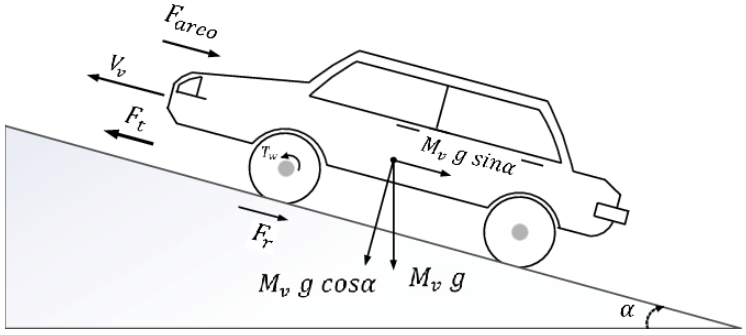

Figure 2.2 : Acting forces on the vehicle.

$$F_{total}=F_r+F_{aero}+F_g+F_m \tag{2.1}$$

For rolling resistance, the equation given in 2.2 is used depending on the speed. Here m is the mass of the vehicle, g is the gravitational acceleration, θ is the slope of the road, and C_0, C_1 and C_2 represent the rolling resistance coefficients. The coefficients considered for C_0, C_1 and C_2 are given in Table 2.1 [15]. Due to the impossibility of precisely predicting these coefficients, their instantaneous variation is analyzed within reasonable values in a random manner. Having the rolling resistance coefficient value exhibit realistic chaos has enabled the vehicle energy consumption outputs to be more in line with real-world data.

$$F_r=mg\left(C_0+C_1\left(\frac{V}{100}\right)+C_2\left(\frac{V}{100}\right)^4\right)cos\theta \tag{2.2}$$

Table 2.1 : Coefficient ranges for rolling resistance [15].

Rolling Resistance Coefficients	Value Range
C_0	0.0072-0.12
C_1	0.00025-0.0028
C_2	0.00065-0.002

The aerodynamic drag force can be expressed by equation 2.3. Here ρ is the air density, C_d is the aerodynamic drag coefficient, A is the frontal area of the vehicle, V is the speed and W is the wind speed [16].

$$F_{aero}=\frac{1}{2}\rho C_d(V\text{-}W)^2 \tag{2.3}$$

Air density is a function of air pressure, relative humidity, and ambient temperature. The effect of relative humidity is negligible [17]. Air density can be determined using the ideal gas law, as shown in equation 2.4. ρ_{air} represents air density, T represents ambient temperature, P_{air} represents atmospheric pressure, and R_{air} represents the specific gas constant for air [17].

$$\rho_{air}=\frac{P_{air}}{R_{air}T} \tag{2.4}$$

$$R_{air}=287.05\frac{J}{kgK} \tag{2.5}$$

According to the study conducted in [16], the variation in air density for different ambient temperatures and air pressures is shown in Figure 2.3. There is an 18% difference between the lowest and highest air density values. In this case, since the aerodynamic drag force can change by 18%, using air density depending on dynamic conditions will enhance the reliability, realism, and consistency of vehicle energy consumption calculations.

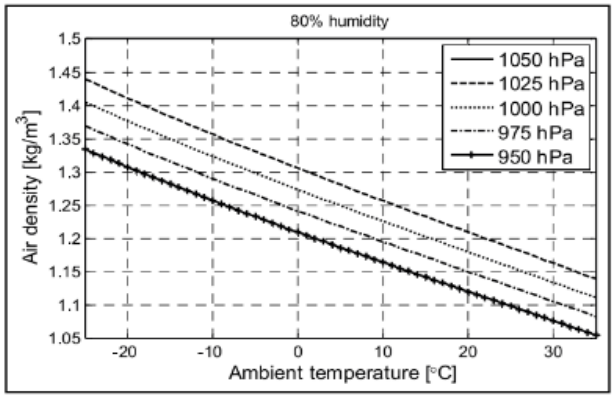

Figure 2.3 : Ambient temperature vs air density graph [16].

The relationship between rolling resistance force and ambient temperature is established using data obtained from tests conducted by the vehicle tire manufacturer Michelin [16]. The graph created based on Michelin's tests is shown in Figure 2.4. Although rolling resistance is not a linear function of ambient temperature, Michelin has suggested that this function be considered linear within the temperature range provided in the graph of Figure 2.4. According to this suggestion, a 1°C change in ambient temperature corresponds to a 0.6% change in rolling resistance force [18].

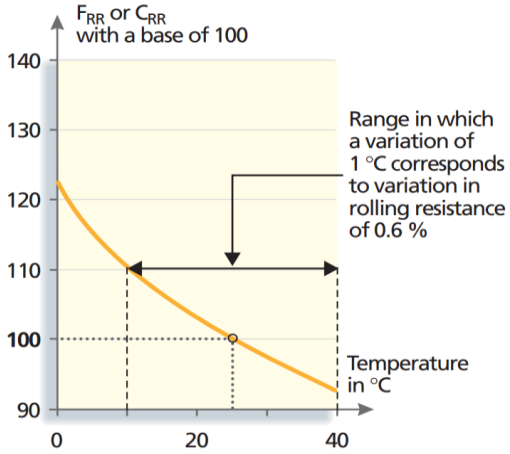

Figure 2.4 : The percentage effect of ambient temperature on rolling resistance force [18].

The acceleration force is given in equation 2.6 [14]. Here, m represents the total mass of the vehicle, a the acceleration, J_w the wheel inertia , J_m the motor inertia, r the wheel radius, and d the gearbox ratio. Depending on the vehicle's deceleration or road slope, the gravitational force can also have a supportive effect in the direction of travel [16].

$$F_m = \left(m + \frac{4J_w}{r^2} + \frac{J_m d^2}{r^2} \right) a \tag{2.6}$$

The total energy consumption of the vehicle over a specific period is obtained by dividing the net energy requirement, calculated by subtracting the energy produced by the vehicle from the total energy required, by the powertrain efficiency [14]. The total energy consumption is given in equation 2.7.

$$E_{tot} = \frac{\int P_{out}(t)dt - \int P_{in}(t)dt}{\eta_{powertrain}} \tag{2.7}$$

EVs benefit significantly from regenerative braking. Unlike internal combustion engine vehicles, EVs act like generators while braking, converting some of the energy that would otherwise be lost as heat back into electrical energy. However, due to the battery's limitations, not all energy can be recovered. The battery's maximum charge current limits how much energy can be regenerated. The energy from regenerative braking can be calculated using equations 2.8, 2.9, 2.10, and 2.11. Here, P_{regen} represents the regenerative braking output power, E_b the energy output from the battery, x the distance, F_{Res} the forces opposing the vehicle's motion, S_v the vehicle's speed, and $n_{powertrain}$ the powertrain efficiency [19].

$$E = \frac{E_b}{x} \tag{2.8}$$

$$E_b = \left(\int_{traction} P_o(\tau)d\tau - \int_{braking} P_i(\tau)d\tau \right) \tag{2.9}$$

$$P_o = \frac{S_V F_{Res}}{\eta_{powertrain}} \tag{2.10}$$

$$P_i = k.P_{regen} \tag{2.11}$$

The driver model is expressed as shown in equation 2.12. *P* and *I* represent the PI controller coefficients. The driver behavior can be modeled by the ability to follow a desired speed profile [14].

$$PI(s)=\left(P+\frac{I}{s}\right) \tag{2.12}$$

2.2 Driving Profile

Worldwide Harmonized Light Vehicles Test Procedure (WLTP) is a test procedure applied for light vehicles worldwide. This procedure is used to evaluate the environmental impact of vehicles and provide more realistic fuel consumption and emission values to the consumer. WLTP replaces older testing methods, more accurately simulating the performance of vehicles in real driving conditions. With this procedure, the fuel consumption and emissions of vehicles in real-world conditions are calculated, taking into account different speed ranges, driving dynamics and stop-start processes [20].

The importance of WLTP increases even more when it comes to electric vehicles. The range and energy consumption of electric vehicles are important decision-making factors for potential buyers. Tests carried out with WLTP make the range and energy consumption values of electric vehicles more transparent and comparable. In this way, consumers can compare different electric vehicle models more consciously and make choices appropriate to actual usage conditions. The speed-time graph of the WLTP drive cycle profile is shown in Figure 2.5.

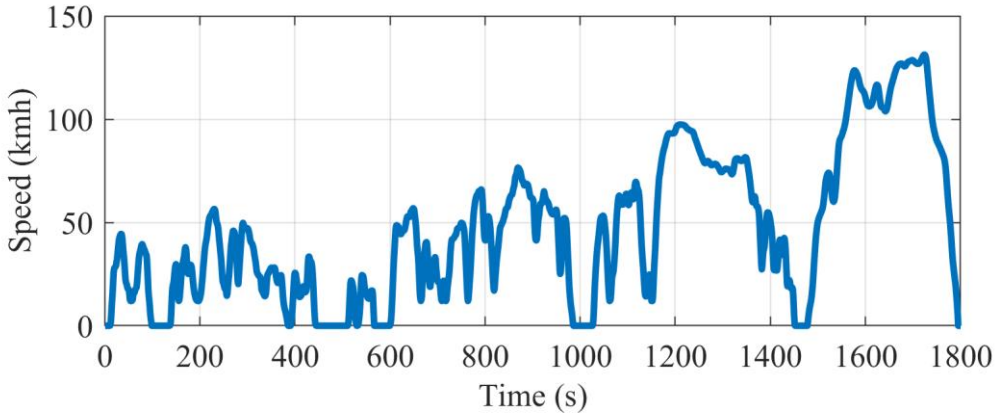

Figure 2.5 :WLTP drive cycle profile.

The WLTP test procedure evaluates different driving conditions of the vehicle under four different scenarios: low, medium, high and very high speed ranges. Each section is designed to test how the vehicle performs in different speed ranges and in different urban and extra-urban conditions. The "low" part simulates short-distance driving at low speeds in urban areas, while the "medium" part represents medium-speed driving on urban and suburban roads. The "High" part measures the vehicle's performance at faster speeds and over longer distances, reflecting urban and highway driving conditions. The “extra high" part tests what kind of energy consumption and emission profile the vehicle has in highway and high-speed situations. The characteristics of the WLTP drive cycle are provided in Table 2.2.

Table 2.2 : WLTP drive cycle specification [21].

	Low	Medium	High	Extra High	Total
Duration (s)	589	433	455	323	1800
Stop Duration (s)	150	49	31	8	235
Distance (m)	3095	4756	7162	8254	23266
% of stops	26.5	11.1	6.8	2.2	13.4
Maximum speed (km/h)	56.5	76.6	97.4	131.3	-
Average speed without stops (km/h)	25.3	44.5	60.7	94	53.5
Average speed with stops (km/h)	18.9	39.4	56.5	91.7	46.5
Minimum acceleration (m/s2)	-1.5	-1.5	-1.5	-1.44	-
Maximum acceleration (m/s2)	1.611	1.611	1.666	1.055	-

2.3 Electric Motor Model

For accurate consumption predictions of an electric vehicle energy consumption model, it requires a dataset that provides high-accuracy electric motor performance predictions. Within the scope of the dynamic model, finite element analyses were applied to the electric vehicle motor of a Nissan Leaf and efficiency maps were derived from the study denoted as [22]. Important data points from the efficiency map shown in Figure 2.6.

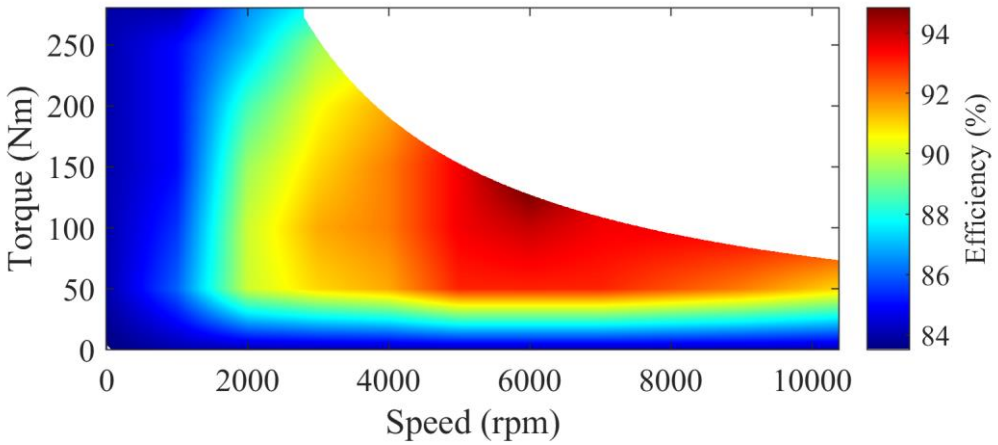

Figure 2.6 : Efficiency map of EV motor.

The extracted data checks the efficiency map based on the speed and torque demanded at the relevant moment of the drive cycle and uses the efficiency map as a look-up table. Subsequently, the efficiency value corresponding to the relevant RPM and torque value will be used to calculate the necessary battery power for the vehicle. Thus, the total energy consumption of the vehicle can be calculated with high accuracy by utilizing the battery power.

2.4 Battery Modelling

The Battery Equivalent Circuit Model (ECM) is a widely used approach to represent the dynamic behavior of batteries. Due to its simple structure and a small number of model parameters, it is extensively used in real-time applications. Instead of detailing the internal structure of batteries physically, ECM represents their electrical characteristics using circuit elements such as resistors and capacitors. Resistors represent the internal resistance and polarization effects of the battery, while the RC network represents the transient state of the battery. This model is used to predict the performance of the battery under various conditions such as voltage, current, and temperature [23].

One of the most commonly used types of ECM in battery modeling is the second-order Thevenin model. The Thevenin model includes a series internal resistance and two parallel RC networks. The series internal resistance models the instantaneous voltage drops of the battery, while the parallel resistor-capacitor network is used to model the time-varying voltage response of the battery. This structure covers both the short-term and long-term dynamics of the battery, representing different behaviors that occur

during charging and discharging [24]. The second-order Thevenin equivalent circuit model is shown in Figure 2.7.

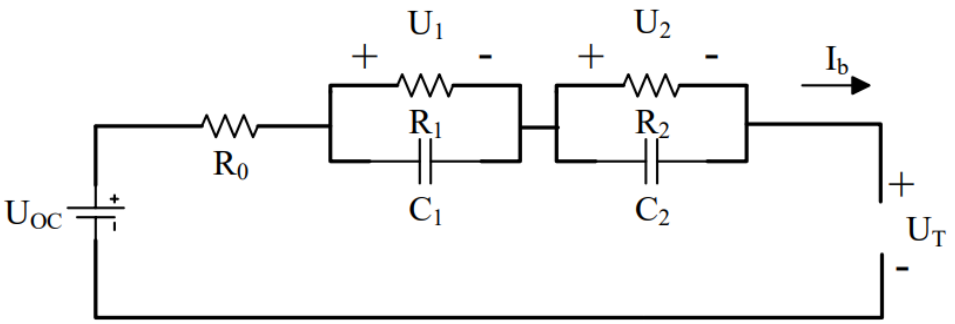

Figure 2.7 : Second-order Thevenin equivalent circuit model.

$$U_1 = -\frac{U_1}{R_1 C_1} + \frac{I_b}{C_1} \tag{2.13}$$

$$U_2 = \frac{U_2}{R_2 C_2} + \frac{I_b}{C_2} \tag{2.14}$$

$$U_T = U_{oc} - U_1 - U_2 - I_b R_0 \tag{2.15}$$

3. BATTERY AGING MECHANISM

With advancing technology, batteries have become an indispensable part of life today. They are used in communication systems, automotive, aviation, and many industrial fields [25,26]. The importance of lithium-ion batteries is increasing day by day due to the need for sustainable technologies and the related development of energy storage systems. In this context, advancements in battery technologies will contribute to the development of more efficient and environmentally friendly energy systems in the future.

Next-generation smart battery management systems, equipped with artificial intelligence technology, can develop models that detect potential errors in advance and delay the battery aging process. These systems are of great importance in critical applications such as performance enhancement, range extension, and battery life extension, especially in electric vehicles. By monitoring and analyzing the health and charge status of batteries in real-time, smart battery management systems develop optimal charging and discharging strategies to extend the life and performance of the battery. Additionally, with increased reliability of fault detection mechanisms, costs can be reduced [27].

The aging and wear processes of lithium-ion batteries and their use under unsafe conditions significantly affect battery performance. When battery performance drops below a certain level, leaks, insulation damages, and partial short circuit problems can have destructive effects on the battery [26]. At this point, the aging mechanism and aging effect are important for battery design and management optimization. From a cell design perspective, the battery aging mechanism and aging model need to be examined, especially in terms of key battery parameters such as energy density and lifespan.

Electrical, mechanical, and thermal effects are critically important in the context of battery aging mechanisms. When examined by battery management systems, the change in the state of battery health over time is a parameter that needs to be modeled and examined in terms of optimizing the current operating state of the battery and

predicting its future performance [25]. On the other hand, the widespread occurrence of fire incidents in products containing LIBs has drawn the attention of the energy sector and the public to the safety of LIBs. Deficiencies encountered in design and production, as well as mechanical, electrical, and thermal problems that may arise as a result of usage, cause failures in LIBs. Additionally, wear factors experienced during actual usage also play a role [28].

Even small-scale advancements aimed at extending battery lifespan will offer significant environmental benefits as the electric vehicle and mobile electronics sectors continue to progress. Understanding the principles of LIB usage and degradation mechanisms contributes to identifying conditions that enhance battery life. The battery management system accurately assesses the functional status of the battery by monitoring parameters such as the state of charge (SOC), state of health (SOH), state of safety (SOS), and state of function (SOF), which are based on measurable outputs like temperature, current, and voltage. This system improves battery performance by providing protection against overcharging and discharging [29].

3.1 General Aging Mechanism

The anode and cathode active materials, separator, and current collectors are the general elements that constitute the layered and electrolyte-filled structure of a lithium-ion battery. The interaction of the anode and cathode active materials with the electrolyte and with each other significantly affects the battery's performance and degradation behavior [30]. The physical and chemical changes of the cell are indicators of the degradation mechanism [31]. The anode and cathode are the parts where most internal aging changes occur [32]. The loss in capacity and power are clear consequences of degradation. The decrease in the usable capacity of the cell and the available power represent capacity and power loss, respectively [31]. On the other hand, the types of reactions and the factors that reduce capacity vary [32].

The reduction in battery capacity during storage occurs in two ways. Reversible and irreversible capacity loss are respectively due to self-discharge and the changes in storage conditions such as temperature, battery SOC before storage, and storage duration. Aging that occurs during battery storage cannot be ignored, as it constitutes 95% of the battery's lifespan [32].

The entire lifespan of a battery is a combination of cycle aging and calendar aging. During cycling, in addition to the main reactions, there are unavoidable side aging reactions that reduce battery power and capacity and increase internal resistance as the number of cycles increases. For electric vehicles, reaching 80% of the nominal capacity generally indicates the end of the battery's life [32].

The formation of the solid electrolyte interphase (SEI) film on the electrode or electrolyte surface, lithium plating, destruction of the electrode structure, phase changes in the electrode material, dissolution of the active material, and electrolyte decomposition all affect battery aging [32]. Lithium inventory loss (LLI), loss of active material at the positive (LAM_{PE}) and negative electrodes (LAM_{NE}), and resistance increase (RI) are the four primary aging modes of aging mechanisms. LLI, which reduces the usable cell capacity, represents the loss of lithium ions through parasitic reactions. LAM_{PE} and LAM_{NE} refer to the insufficiency of active material used for lithium added to the cathode and anode. The cell's resistance or impedance increases with RI, leading to a decrease in power. Additionally, it causes a reduction in usable capacity when the charge and discharge cut-off voltage do not change [30]. The production of SEI, overvoltages, extreme temperatures, lithium plating, or the reaction of moisture contamination with hydrofluoric acid (HF) formation are various causes leading to electrolyte loss at the interfaces of both electrodes, which is a significant factor in impedance increase [31].

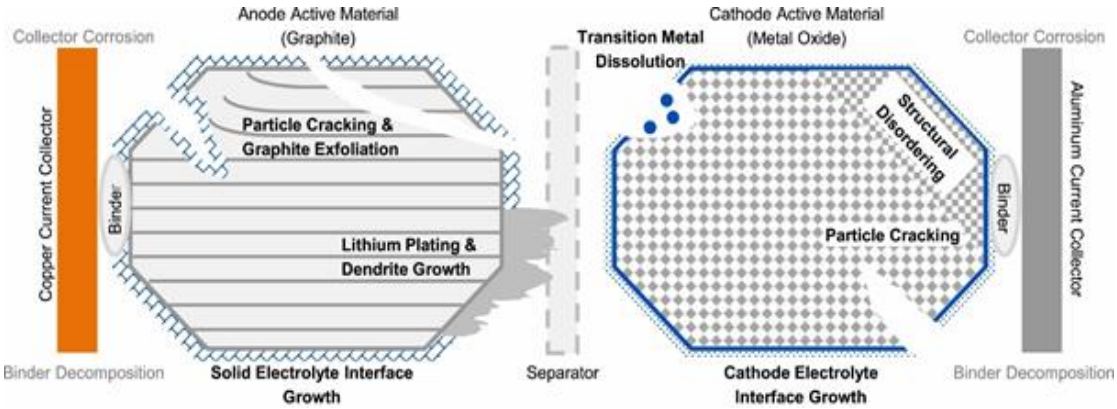

Figure 3.1 : Battery aging mechanism [30].

3.2 Cathode Aging Mechanism

Irreversible phase changes can be observed with the intensification of battery aging in the cathode material. Irreversible capacity degradations can result from excessive

mechanical stress caused by certain phase changes [32]. The exacerbation of side effects is also related to the significant increase in temperature due to high currents during battery loading conditions and operation at high current rates [33]. Particle detachment, structural degradation, particle cracking, structural disintegration, transition metal dissolution, and the formation of the cathode-electrolyte interface are mechanisms that are prominent in the cathode, especially concerning metal oxides [30]. The dissolution of cathode materials, mainly due to the transport and accumulation of soluble substances in the anode, is the primary factor reducing the battery's cycle life. The increase in the transition metal layer's interface hinders the diffusion of lithium ions and the rise in battery polarization, leading to reduced battery capacity as some lithium ions cannot intercalate, resulting in structural damage [32]. Particle fracture, seen in the anode, is caused by volume changes during the charging and discharging cycles, damaging the cathode material's structure and leading to the loss of active material (LAMPE) [25,30]. The cracking of cathode material is a result of operating the battery under high voltage or current conditions over extended cycles [33]. Furthermore, trapped lithium causes LLI in addition to LAMPE due to contact loss during the lithiation of cathode active material. The structural disorder leading to LAMPE and RI is a reaction resulting from the substitution of Li+ ions with transition metal ions within the lattice. The cathode-electrolyte interface forms similarly to SEI when the cathode reacts with the electrolyte [30]. The passivation layer, also known as the cathode electrolyte interface (CEI) film, does not have to be thicker than SEI to cause RI and LAMPE [30,32]. The increase in interface resistance and the intensification of cathode polarization result from the expansion of the CEI film on the cathode/electrolyte surface due to the increased number of battery cycles [32]. High temperatures accelerate electrolyte decomposition, facilitating CEI formation [33]. Additionally, LAMPE may result from the dissolution of transition metals from the cathode to the electrolyte. SEI formation is said to increase as the dissolved metal migrates to the anode [30]. The decomposition and loss of electrolyte, phase changes in the lattice, binder decomposition due to high temperatures, and the erosion of the current collector are other identified degradation mechanisms for the cathode [30,33]. The erosion of the binder, leading to increased battery internal resistance due to loss of contact between the electrodes, destabilizes the positive electrode structure [33]. The factors occurring in the cathode are shown in Figure 3.2.

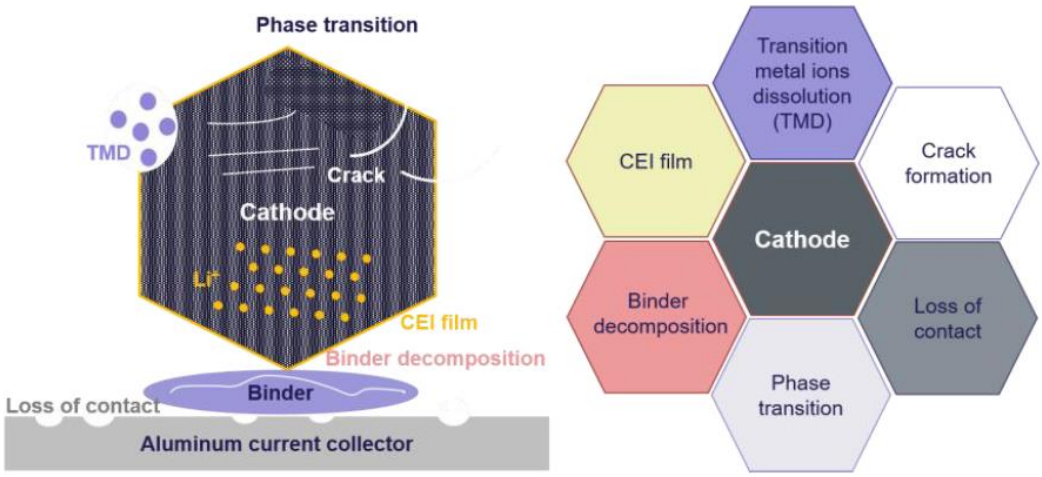

Figure 3.2 : Degradation mechanisms occurring in the cathode [33].

3.3 Anode Aging Mechanism

While carbon, graphite, titanate, and silicon are preferred in battery chemistries, graphite holds a significant place concerning battery reliability and aging [34]. One of the predominant causes of anode aging is the reactions occurring at the interface between the electrolyte and the negative electrode. These reactions lead to the loss of electrolyte and active lithium ions. The products of these reactions accumulate on the surface of the negative electrode, forming a layer known as the Solid Electrolyte Interphase (SEI) layer [34,35]. The initial formation of the SEI layer can be described as the reduction of the electrolyte on the anode surface during the battery's first charge. This stage consumes approximately 10% of the active lithium ions, beginning to challenge the necessary anode-cathode capacity ratio essential for battery performance. The stability and compactness of the SEI layer are significantly affected by the electrode and electrolyte solution used in the battery and by external factors such as temperature and current. Proper selection of the battery structure along with appropriate temperature and current values is crucial for performance and aging [32]. The SEI layer is one of the primary causes of capacity and power loss in the battery aging mechanism. Throughout the battery's lifespan, this layer grows, and solvent molecules can permeate the layer. As a result, cracks can form on the anode surface experiencing volume expansion, which can increase the surface area for further SEI formation [30]. The growing SEI layer depletes the active lithium ion reserves in the battery, increasing electrode impedance and leading to capacity and power loss [34].

Another factor effective in anode aging is lithium plating. Factors that lead to lithium plating include low temperature, high state of charge, high charging current, and high cell potential. Lithium plating occurs when active lithium ions form a plate on the surface instead of intercalating into the negative electrode. This plating supports the formation of the SEI layer, leading to a reduction in the electrolyte solvent [31]. Contrary to the formation principle of the SEI layer, this results in a decrease in the active electrode surface area, increasing the current density passing through the remaining surface pores. This situation endangers battery safety by increasing the likelihood of short circuits within the battery, consequently promoting further metal plating [36]. This process, which contributes to SEI layer formation and consumes active ions, also leads to a decrease in battery capacity and power [34]. In battery aging curves, the impact of lithium plating typically manifests as a knee point in the behavior [36]. The aging stages on the negative electrode are shown in Figure 3.3.

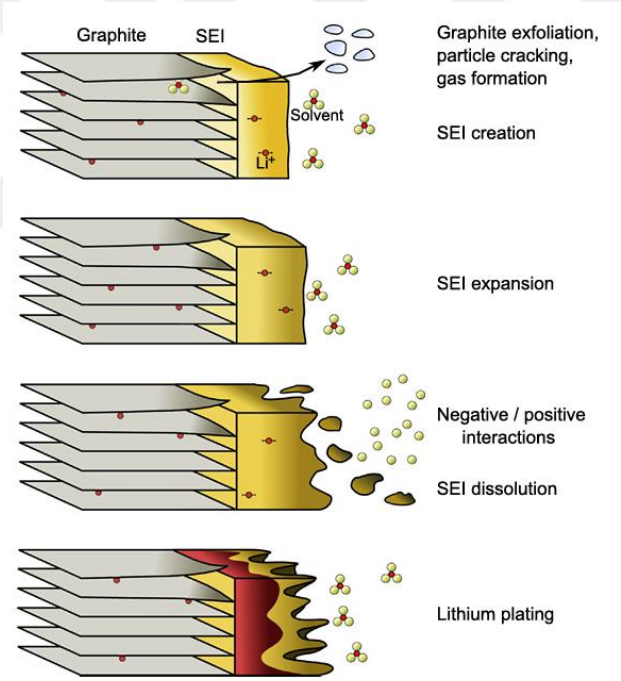

Figure 3.3 : Aging effects on the negative electrode [34].

Mechanical and electrical contact losses occurring in the anode are also among the factors contributing to anode aging. The primary factor leading to contact loss is the increase in active anode material. Volume and structural changes in the active material significantly affect the permeability of the electrode, reducing anode performance and leading to capacity loss [34].

3.4 Lithium Iron Phosphate Battery Degradation Model

The aging models of LFP (Lithium Iron Phosphate) batteries are critical for optimizing the performance and lifespan of energy storage systems. Battery aging models help understand the chemical and physical changes that batteries undergo throughout their usage period. These models can be used in battery design, management, and predictive maintenance strategies. Empirical models predict battery aging based on historical data and experimental results. These models typically use statistical relationships derived from data collected under specific usage conditions.

3.4.1 Lithium iron phospate battery cycle aging model

Wang et al. [37] have developed a semi-empirical battery aging model by curve fitting experimental data on the cyclic aging of lithium iron phosphate cells. With the developed model, a connection has been established between capacity degradation and parameters such as C-rate, temperature, and Ah-throughput. In equation 3.1, Q_{loss} represents the capacity reduction, B the pre-exponential factor, E_a the activation energy, R the gas constant, T the temperature in Kelvin, A_h the ampere-hour throughput, and z the power law factor.

$$Q_{loss}=B.\ exp\left(\frac{-E_a^{'}}{RT}\right)A_h^z \tag{3.1}$$

Ah-throughput is expressed as the product of the number of cycles (N), the battery capacity (C), and the Depth of Discharge (DoD) in equation 3.2. Equation 3.3 expresses the relationship between the activation energy and the C_{rate}. Here, the constant c is 370.3.

$$A_h=N.C.DoD \tag{3.2}$$

$$E_a^{'}=31700-c.C_{rate} \tag{3.3}$$

Based on the experimental results by Shen et al [38], a curve fitting method was employed using the pre-exponential factor provided for four distinct C_{rate} values, facilitating the computation of the B value for different C_{rate} values. The equations of the fitted curve and its parameters are presented in equations 3.4 and 3.5.

$$lnB=a.e^{(-\lambda.C_{rate})}+d \tag{3.4}$$

$$a=1.226,\ \lambda=0.2797,\ d=9.263 \tag{3.5}$$

3.4.2 Lithium iron phospate battery calendar aging model

Battery calendar aging describes the process where storage duration, environmental conditions, and the state of charge (SoC) during storage lead to a reduction in battery capacity and performance. [39] conducted calendar aging tests on a 2.3 Ah capacity Lithium Iron Phosphate battery cell. In this study, aging data obtained from maintaining the battery under various temperature and Stateof-Charge (SoC) conditions were analyzed. As a result of the analyses, an empirical formula was developed to predict the aging process of the battery. The derived empirical formula and its coefficients are shown in equations 3.6, 3.7, 3.8, and 3.9, respectively.

$$Q_{cal} = A(SoC) \cdot exp\left(\frac{B(SoC)}{RT}\right) \cdot t^{C(T)} \tag{3.6}$$

$$A = 0.2433 \cdot SoC^3 + 0.0476 \cdot SoC^2 + 0.2993 \cdot SoC \tag{3.7}$$

$$B = -10.294 \cdot SoC^3 + 21.229 \cdot SoC^2 - 0.7797 \cdot SoC \tag{3.8}$$

$$C = -1.8157 \cdot 10^{-7} \cdot T^3 + 1.3449 \cdot 10^{-4} \cdot T^2 - 0.0226 \cdot T \tag{3.9}$$

The comparison of the experimental results and the model results is presented in Figure 3.4.

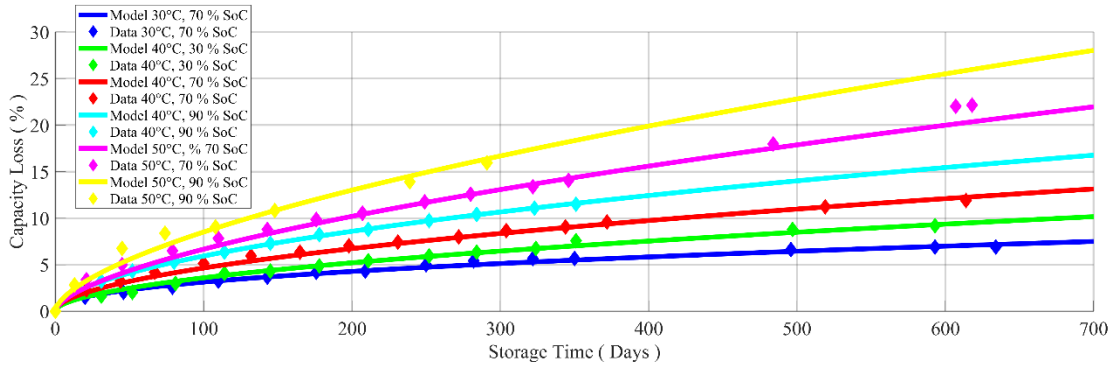

Figure 3.4 : Battery calendar aging graph.

3.5 Nickel Manganese Cobalt Battery Degradation Model

Wang, in his previous studies [37], proposed a cycle aging model for lithium iron phosphate (LFP) type battery cells. In this study, an aging model has been developed for a 1.5 Ah capacity 18650 LMO-NMC type battery cell produced by Sanyo technology. Various parameters were examined using electrochemical methods during the battery life tests. Data such as capacity loss, voltage drop, resistance increase, lithium loss, and active material loss revealed that factors such as the number of cycles, temperature, and depth of discharge significantly affect battery performance. The developed calendar life loss model bases the parameters of the capacity loss equation on a fitting model that assumes an Arrhenius dependency [40]. This model can be used to determine the capacity loss experienced by the battery over its usage period. The aging model due to calendar aging is shown in equation 3.6.

$$Q_{loss,calendar} = A \cdot exp\left(\frac{-Ea}{R \cdot T}\right)(t)^{0.5} \tag{3.6}$$

Here, empirical equations expressed with the parameters determined as A pre-exponential factor, E_a activation energy, R gas constant, and T temperature were used. The coefficients obtained by fitting the experimental data to these equations through curve fitting are shown in equation 3.7 [40]. The model results and experimental data are shown comparatively in Figure 3.5.

$$Q_{loss,calendar} = 14876 \cdot exp\left(\frac{-24.5kJ}{R \cdot T}\right)(day)^{0.5} \tag{3.7}$$

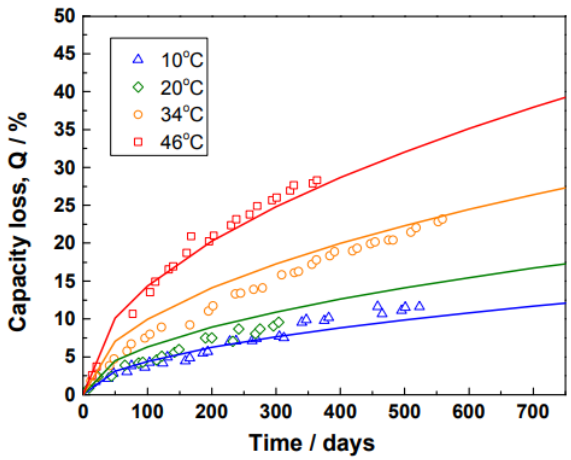

Figure 3.5 : Comparison of Experimental and Model Results for Calendar Aging [40].

The cycle aging model was developed using data obtained under the condition of 50% depth of discharge. The model is based on data from experiments conducted at different temperature values using the same approach. In equation 3.8, β_1 is the pre-exponential fitting factor, β_2 is the exponential fitting factor, and Crate represents the current rate.

$$Q_{loss,cycle} = \beta_1 \cdot exp(\beta_2 \cdot rate) Ah_{throughput} \quad (3.8)$$

The model parameters under different temperatures are provided in Table 3.1.

Table 3.1 : Cycle Aging Model Parameters under Different Temperatures [40].

Temperature	Cycle Aging Model
10°C	$[0.0021 \cdot \exp(0.4278 \cdot \text{rate})].\text{Ah}_{\text{throughput}}$
20°C	$[0.0008 \cdot \exp(0.3903 \cdot \text{rate})].\text{Ah}_{\text{throughput}}$
34°C	$[0.0010 \cdot \exp(0.3107 \cdot \text{rate})].\text{Ah}_{\text{throughput}}$
46°C	$[0.0045 \cdot \exp(0.1826 \cdot \text{rate})].\text{Ah}_{\text{throughput}}$

The generalized cycle and calendar aging function is given in equation 3.9.

$$Q_{loss} = (a \cdot T^2 + b \cdot T + c) \cdot exp[(d \cdot T + e) \cdot I_{rate}] \cdot Ah_{throughput} + f \cdot t^{0.5} \cdot exp[-\frac{E_a}{R \cdot T}] \quad (3.9)$$

Accordingly, the generalized cycle and calendar aging model parameters are provided in Table 3.2.

Table 3.2 : Model Parameters

Symbol	Value
a	$8.61e^{-6}$
b	$-5.13e^{-3}$
c	$7.63e^{-1}$
d	$-6.7e^{-3}$
e	2.35
f	14.876
I_{rate}	C_{rate}
t	Day
E_a	14.876
R	8.314
T	Kelvin

4. BATTERY SELECTION OF ELECTRIC VEHICLE

The performance, range, and cost of electric vehicles significantly depend on the characteristics of the battery cells used. Therefore, during the selection of battery cells, it is essential to consider factors such as cost, volume, weight, and especially battery life. The cost of battery cells constitutes a significant portion of the overall vehicle cost. The volume and weight of the battery pack, obtained by connecting cells in series and parallel, play a decisive role in the vehicle's energy consumption and hence its range. Additionally, the rate of cell aging is a critical factor directly affecting the overall service life of the electric vehicle and its maintenance costs.

In this study, a comparative analysis of lithium iron phosphate battery cells, which are commonly used in electric vehicles, is presented. A detailed examination is conducted on a battery pack with a capacity of 40 kWh. This study involves the design of four different LiFePO4 battery cells and compares them in terms of weight, volume, price, and aging aspects of the battery pack. With this study, which emphasizes the importance of cell selection in electric vehicles, it becomes possible to design battery packs that are longer-lasting and more economical.

4.1 Scenario

It is assumed that an electric vehicle completes five WLTP driving cycles per day, and during this process, four different battery packs are examined. The analysis includes the battery cell currents during each WLTP cycle, the vehicle's total energy consumption after five cycles, and SoC values. Additionally, the battery aging rates at the end of a ten-year usage period and the total WLTP range that the vehicle can cover from 100% to 0% SoC have also been evaluated. The system block diagram is shown in Figure 4.1. A battery pack with a capacity of 40 kWh and a voltage of 400V has been designed for each battery cell. Battery cells vary in capacity and size, leading to significant variations within the battery pack. Accordingly, the calculation of the number of cells connected in series is given in equation 4.1, the calculation of the number of parallel branches in equation 4.2, the total battery pack mass calculation in equation 4.3, and the total battery pack volume calculation in equation 4.4.

The block diagram of the system was shown in Figure 4.1.

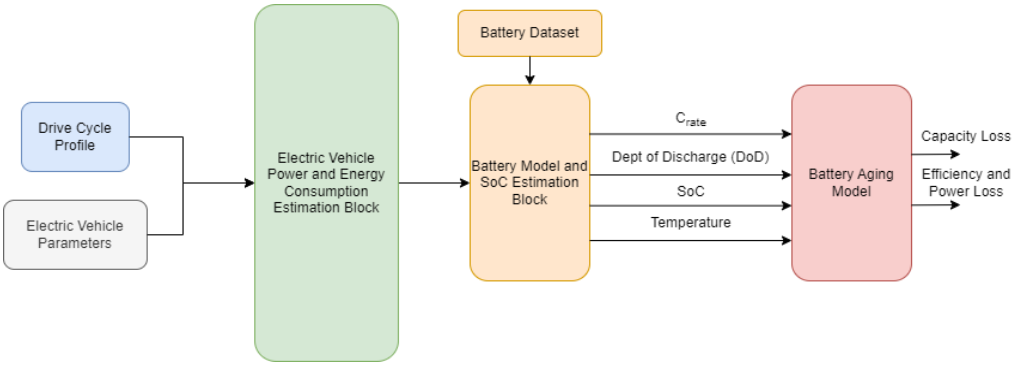

Figure 4.1 : System block diagram.

$$Number\ of\ Series\ Cel\ l = s = \frac{Battery\ Pack\ Voltage}{Cell\ Voltage} \tag{4.1}$$

$$Number\ of\ Parallel\ Cell = p = \frac{Battery\ Pack\ Capacity}{Cell\ Capacity \cdot Cell\ Voltage \cdot Number\ of\ Series\ Cell} \tag{4.2}$$

$$Battery\ Pack\ Mass = s \cdot p \cdot Cell\ Weight \tag{4.3}$$

$$Battery\ Pack\ Volume = s \cdot p \cdot Cell\ Size \tag{4.4}$$

4.2 Validation of Battery Degradation Model

To validate the accuracy of the battery aging model, the model outputs were compared with the cycle aging results specified in the battery cell datasheets. This comparison was performed under various operating conditions and different cycle numbers. As a result, the battery aging process was modeled within a 2% error margin. The specifications of the battery cells are provided in Table 4.1.

Table 4.1 : Battery Cell Specifications.

	Cell – 1 [41]	Cell -2 [42]	Cell – 3 [43]	Cell – 4 [44]
Manufacturer	A123 Systems	A123 Systems	Cegasa Portable Energy	A123 Systems
Type	LFP	LFP	LFP	LFP
Capacity (Ah)	1.1	2.3	3.2	20
Nominal Voltage (V)	3.3	3.2	3.2	3.3
Volume (cm^3):	16.5	34.5	34.5	263.3
Weight (g)	39	70	86	495
Price (p.u)	2.16	5.3	1	11.6

The aging graphs and error rates of the batteries are shown in Figures 4.2, 4.3, 4.4, and 4.5, respectively.

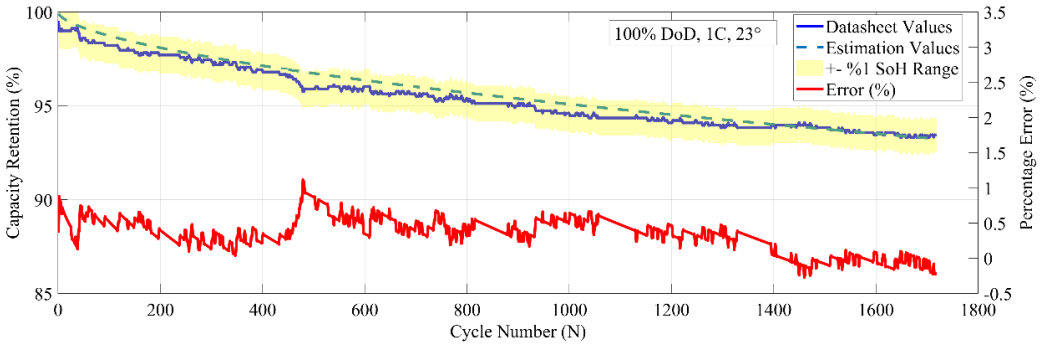

Figure 4.2 : 1.1 Ah battery degradation model.

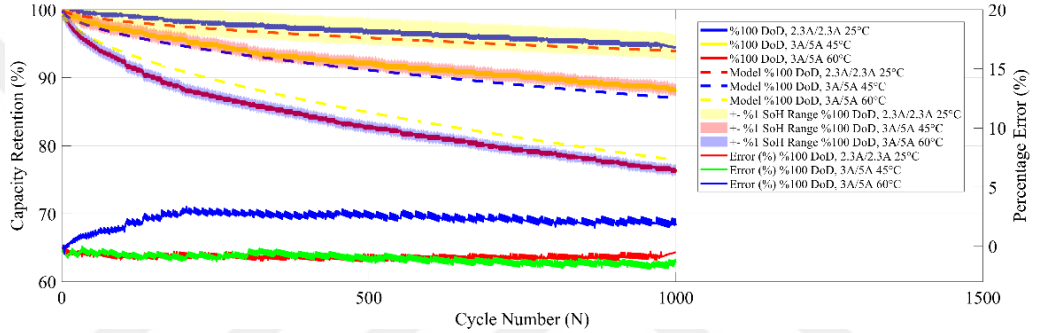

Figure 4.3 : 2.3 Ah battery degradation model.

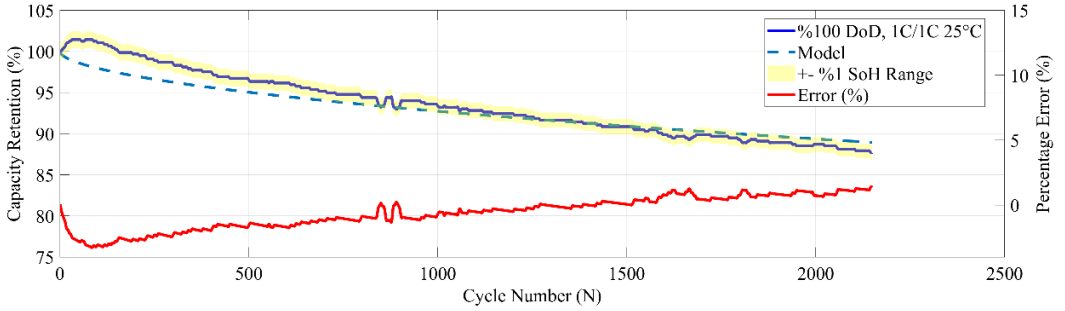

Figure 4.4 : 3.2 Ah battery degradation model.

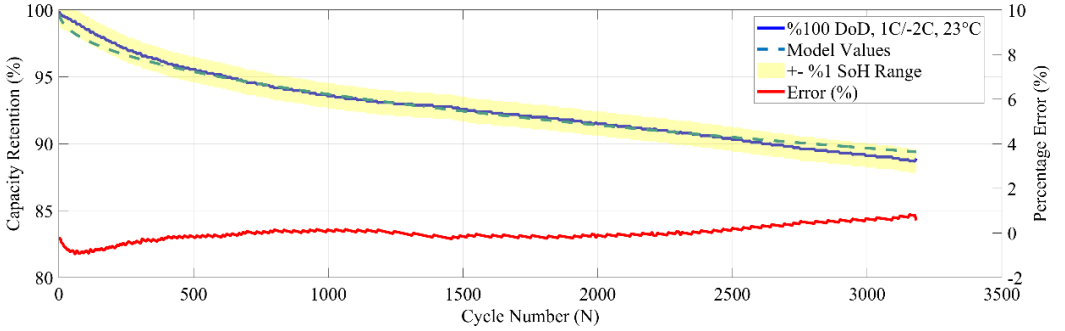

Figure 4.5 : 20 Ah battery degradation model.

4.3 Battery Selection Algorithm

In the Battery Selection algorithm, a battery pack with a capacity of 40 kWh and a nominal voltage of 400V per cell has been designed. These battery packs were tested using 5 WLTP driving cycles integrated into the electric vehicle model. As a result of these tests, the energy consumptions at the end of the driving cycle, SoC changes, vehicle ranges, and the aging status of the batteries over a 10-year usage period were examined for each battery pack, and the effects of this aging on battery performance were evaluated. The weight, volume, price, and battery aging data of the battery packs were subjected to a normalization process. This normalization process was carried out to enable a fair comparison of battery packs with different characteristics. As a result of the normalization process, the weight, volume, price, and aging rates of each battery pack were made comparable. In the final stage, a cost function was created to be used in the selection of battery packs. This function was optimized by evaluating battery aging at 50%, weight at 20%, price at 20%, and volume at 10%. The cost function is shown in equation 4.5.

$$F(x)=0.5 \cdot f_{aging}(x)+0.1 \cdot f_{volume}(x)+0.2 \cdot f_{price}(x)+0.2 \cdot f_{weight}(x) \quad (4.5)$$

The battery selection algorithm flowchart is shown in Figure 4.6.

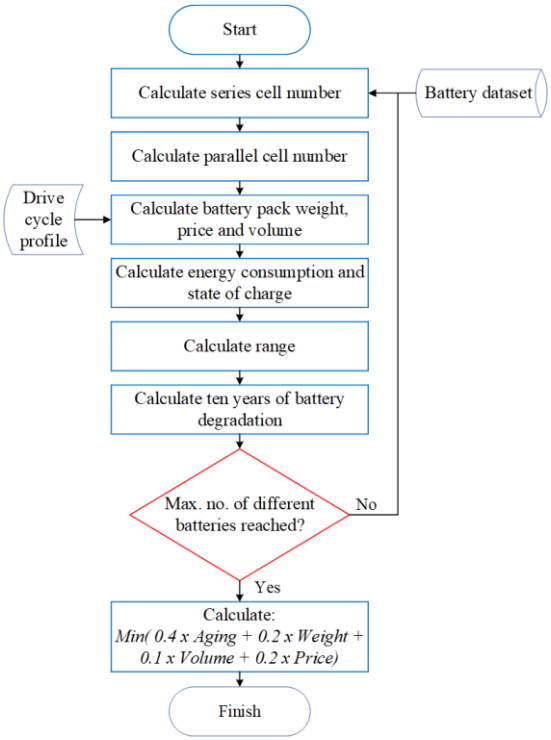

Figure 4.6 : Battery selection algorithm flowchart.

5. ANALYSIS AND OPTIMIZATION OF VEHICLE TO GRID SERVICES

Vehicle-to-Grid technology is a smart grid concept that enables electric vehicles to establish bidirectional communication with power grids, providing benefits to both the grid and electric vehicle drivers while having the potential to improve the overall operation of the grid. Seen as a crucial component of future sustainable energy systems, this technology allows electric vehicle batteries to quickly supply additional power to the grid during periods of fluctuating energy demand, reduce stress on transmission lines, and regulate frequency and voltage variations [45,46]. Thus, the efficiency and reliability of the system can be enhanced, the need for infrastructure investments can be reduced, resulting in cost savings for both energy companies and users, and grid stability can be supported.

5.1 Benefits of the Provided Services for the Grid

Electric vehicles can offer comprehensive services to meet the needs of the grid. Transmission congestion occurs when a specific transmission line lacks the capacity to meet the current demand. This happens when the flow of electricity from generation points to consumption points exceeds the capacity of the existing transmission lines. In such cases, the batteries of electric vehicles can supply their stored energy to the grid, reducing the stress on the transmission line. This helps alleviate congestion and supports the grid [47].

The frequency of the electricity grid changes based on the balance between energy demand and production. It is necessary to ensure that the total generation in the system perfectly matches the total load at all times. Maintaining a stable frequency is crucial for preserving this balance and ensuring the efficient and safe operation of the power grid.

Frequency regulation involves using the batteries of electric vehicles to supply extra energy to the grid during high demand periods or storing energy when demand is low [48].

By assisting with peak demand during high demand periods, electric vehicles use their batteries as energy storage units, allowing for more efficient use of the existing grid infrastructure and reducing the costs of new infrastructure investments such as additional transmission lines and transformers. Additionally, it optimizes grid management and energy distribution, thereby increasing operational efficiency [49]. The types of V2G services are shown in Figure 5.1.

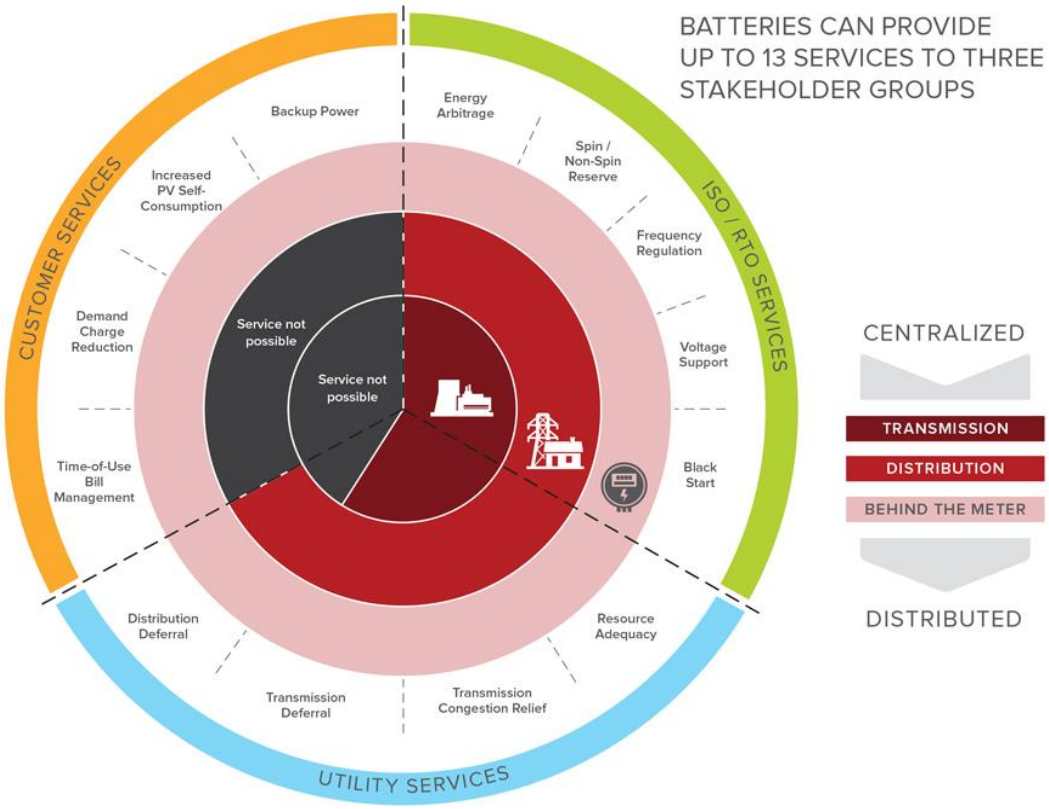

Figure 5.1 : An overview of the services provided by V2G technology [50].

5.2 Benefits of Provided Services for Users

Among the benefits that Vehicle-to-Grid services offer to electric vehicle users is the significant reduction in charging costs. By charging electric vehicles during nighttime, when demand is low, users can take advantage of lower tariffs, thereby reducing their charging costs, while energy companies also benefit from reduced operational costs during these periods [49]. This helps to minimize energy losses and maintain the power system's operational capacity at lower levels, thereby reducing total power losses [51]. Additionally, the services provided to the grid allow electric vehicle users to sell electricity back to the grid at higher tariffs during periods of high demand [51].

5.3 Selection of Grid Frequency Data Using K-means Clustering Algorithm

The k-means clustering or classification algorithm is a type of algorithm used to partition data from complex and large datasets into similar clusters. It is widely used in fields such as machine learning, statistics, and psychology, where complex datasets are common [52]. Clustering similar data points and keeping each cluster distinct from one another facilitates the interpretation and analysis of the dataset [45]. The algorithm essentially calculates the distance of each data point to the centroids of k clusters, which are initially assigned randomly. The goal is to create k distinct clusters that encompass the entire dataset and minimize the distances of data points within each cluster to their respective centroids. Iterations continue until these distance values reach a minimum [46].

Grid frequency data from Great Britain has been used for planning vehicle-to-grid services. To create a realistic scenario, one year of grid frequency data was analyzed using the k-means algorithm, and 10 days with the most distinct characteristics were selected. This selection was made by leveraging the algorithm's ability to minimize similarities between clusters. The selected 10 days were then used in various combinations to generate a 10-year dataset.

However, due to the k-means algorithm producing different results each time it is run, 5000 iterations were performed to increase the accuracy of this process. Since each iteration was based on random starting points, different combinations of days emerged. To obtain the most statistically significant and diverse dataset, the combination with the highest variance from these 5000 iterations was chosen, and analyses were conducted on these days.

The selected days, considering the percentage sizes of the clusters, were used to generate a ten-year grid frequency dataset. The number of days in the ten-year dataset was distributed according to the same percentage sizes of the clusters. This derivation process was carried out based on the available one-year frequency data, aiming to reflect long-term scenarios more realistically. The days obtained by the k-means clustering algorithm and the percentage distributions of the clusters are shown in Figure 5.2. The total 30-minute Δf values of the selected days for the threshold values of 49.985 – 50.015 Hz are shown in Figure 5.3.

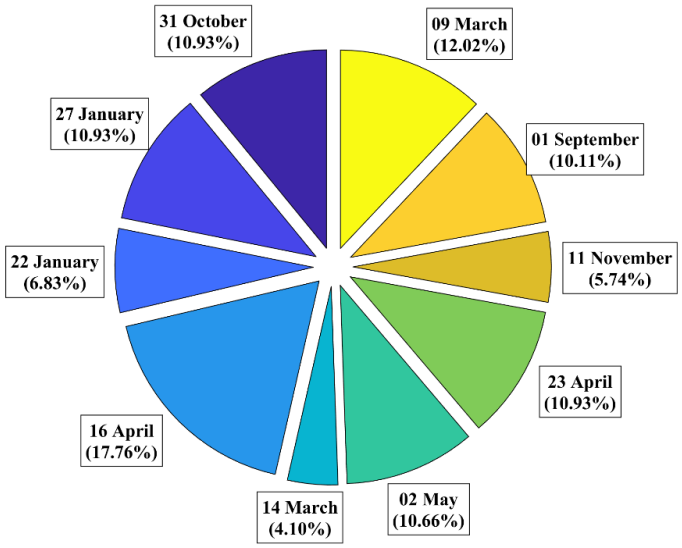

Figure 5.2 : Selected days and distribution of cluster sizes.

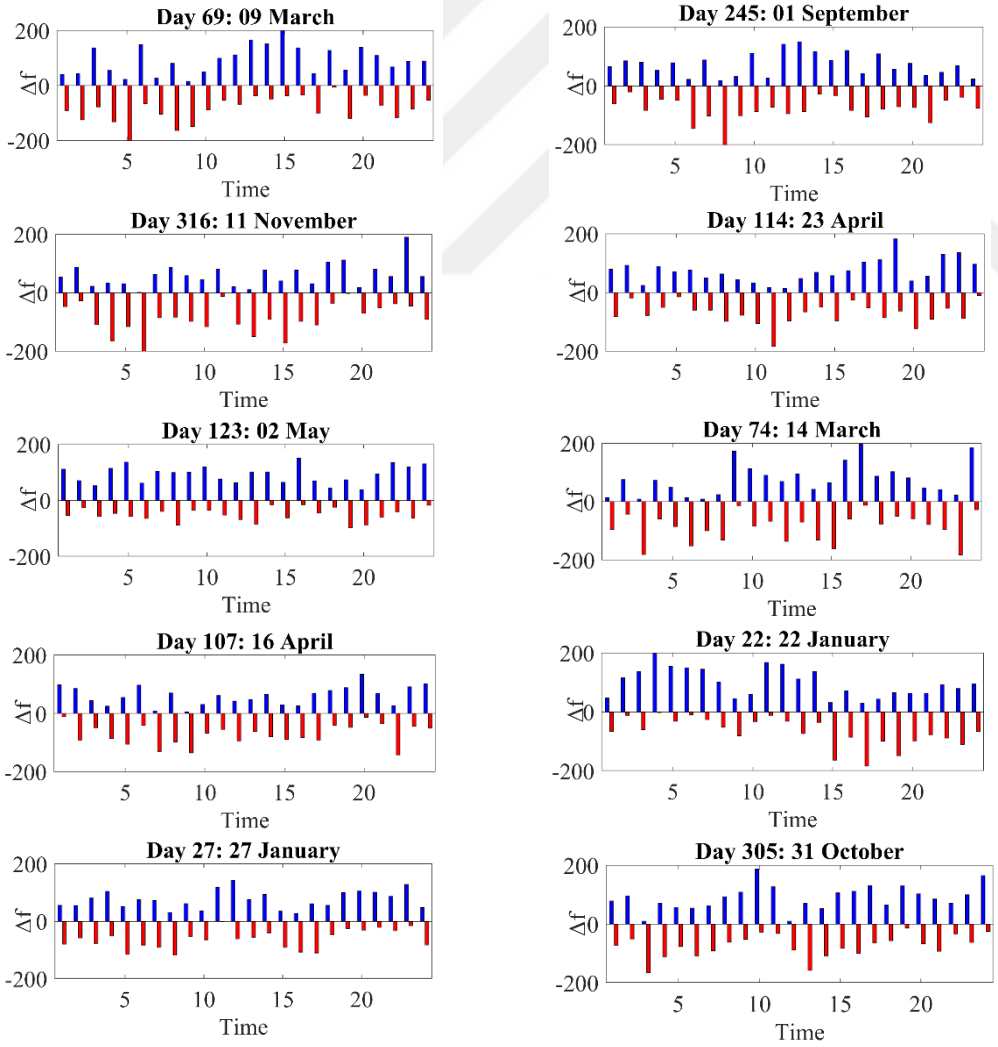

Figure 5.3 : The total Δf values of the selected days with the threshold frequency value.

The selected days are given in Figure 5.4.

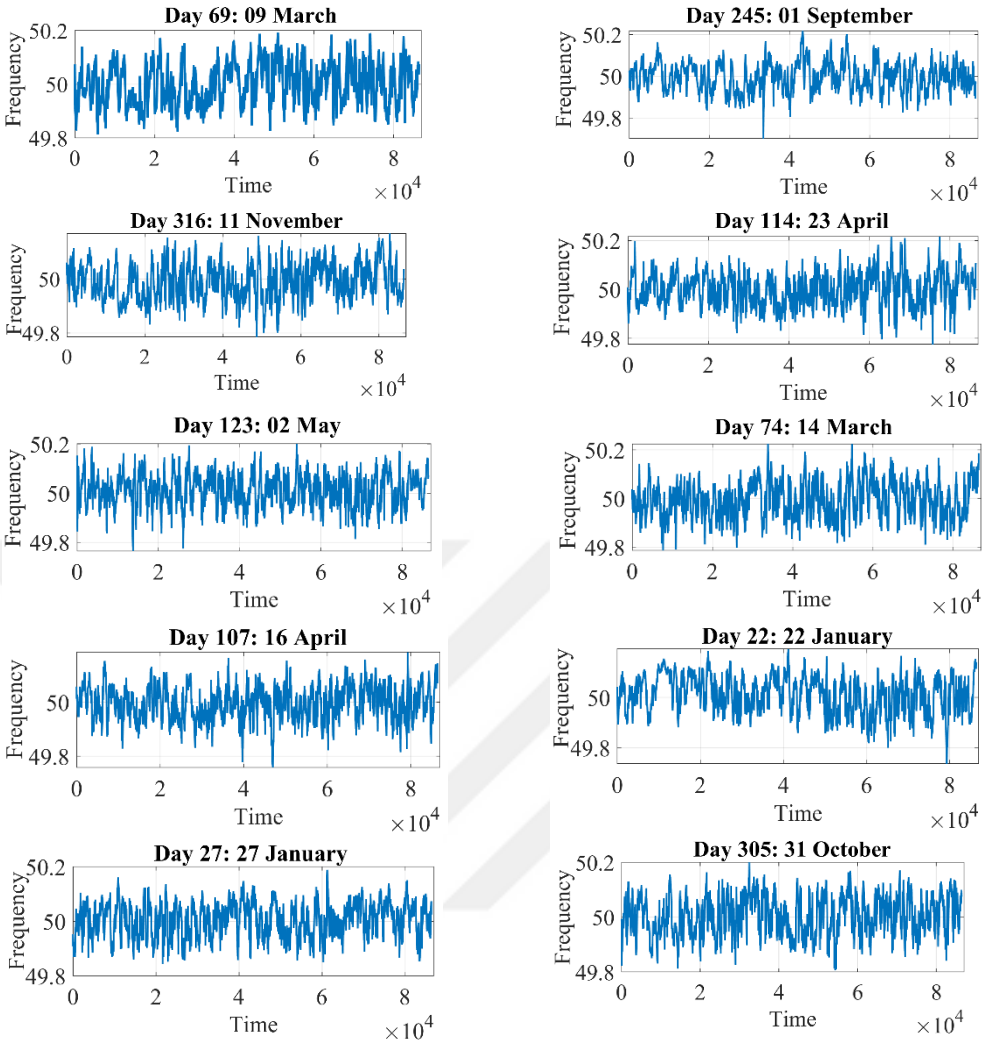

Figure 5.4 : The grid frequency values of the selected days.

5.4 Scenario and Optimization Algorithm

In the developed electric vehicle model, grid frequency data from Great Britain were used for vehicle-to-grid service planning. Daily frequency data were divided into thirty-minute periods, and optimization was carried out using a binary genetic algorithm with various weights given in terms of the electric vehicle's revenue and battery aging. The binary genetic algorithm is a method where decision variables are represented in binary form and are evolutionarily optimized through genetic operators. This algorithm is population-based, with each individual evaluated as a proposed solution. New generations are created using operators such as selection, crossover, and mutation, evolving towards the best solution. The flowchart of the binary genetic algorithm is shown in Figure 5.5.

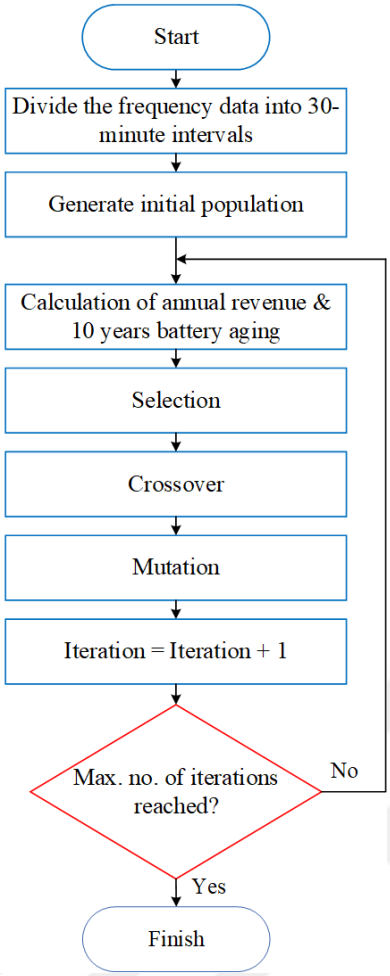

Figure 5.5 : Flowchart of optimization algorithm.

As a scenario, the electric vehicle makes two trips every day. One trip occurs at 09:00 in the morning, and the other at 18:00 in the evening, each lasting thirty minutes. During each trip, the vehicle travels a total of twenty-three kilometers. The vehicle is charged every night between 23:00 and 23:59 and starts each day with an 80% state of charge. It is assumed that the vehicle is available to provide V2G frequency regulation services during the remaining time. The V2G service can operate bidirectionally when the state of charge is between 90% and 40%. If the state of charge is above 90%, the battery can only discharge through the V2G service. When the state of charge falls below 40%, the battery can only be charged through the V2G service. The optimization algorithm decides whether or not to provide vehicle-to-grid service during different periods of the day based on various weights. An optimal strategy is developed in accordance with grid demands and the vehicle owner's revenue expectations. In the study, a total of six different scenarios were examined. Among these scenarios, the effects of different charging station powers, specifically 11 kW and 3.7 kW, on

revenue and battery aging were comparatively analyzed. For each charging power, optimal results were obtained that minimize battery aging, maximize revenue, and balance 50% revenue with 50% battery aging.

The critical frequency values required for frequency regulation will be determined by a piecewise function, referred to as y_t as given in equation 5.1 [53].

$$y_t = \begin{cases} f_t < 49.8\ Hz, -1 \\ 49.8\ Hz \leq f_t < 49.985\ Hz, (f_t\text{-}50)/0.2 \\ 49.985\ Hz \leq f_t \leq 50.015\ Hz, 0 \\ 50.015\ Hz < f_t \leq 50.2\ Hz, (f_t\text{-}50)/0.2 \\ f_t > 50.2\ Hz, 1 \end{cases} \tag{5.1}$$

The critical frequencies of the grid have been determined through the y_t piecewise function. The distance of the instantaneous frequency value f_t from the nominal grid frequency value of 50 Hz determines the output of the y_t function. For frequency values below 49.8 Hz, power will be supplied to the grid at P_{Charge}, and for frequency values above 50.2 Hz, power will be drawn from the grid at P_{Charge}. For intermediate values such as 49.8 Hz ≤ f_t < 49.985 Hz and 50.015 Hz < f_t ≤ 50.2 Hz, the ratio $\frac{f_t-50}{0.2}$ will be used. For frequency values between 49.985 Hz and 50.015 Hz, no frequency regulation is required. The power value that the vehicle will use for V2G or G2V operations is given in equation 5.2. The P_{charge} value has been compared for 3.7 kW and 11 kW.

$$P_{V2G} = y_t \cdot P_{Charge} \tag{5.2}$$

6. RESULT AND DISCUSSIONS

6.1 Battery Selection Algorithm Results

The study conducted in Section 4 resulted in the creation of 4 different vehicle models using each battery cell. For each model, the battery cell current, distance, energy consumption, SOC, and SOH values of the vehicles were compared over 5 WLTP driving cycles. At the end of the evaluation, the optimal battery cell selection in terms of battery aging, weight, volume, and price was carried out according to the cost function in equation 4.5.

The differences in weight have a significant impact on energy consumption in the 40 kWh battery packs created using four different battery cells. Each battery cell's varying mass directly affects their energy consumption profiles. In the heaviest battery pack, energy consumption was at its highest level due to the need to carry more mass. This negatively impacts vehicle performance, leading to higher energy expenditure.

On the other hand, the lightest battery pack provided the lowest energy consumption due to having less mass to carry during transportation. Less weight facilitates the vehicle's movement, increasing energy efficiency. This has a positive effect on the overall efficiency and lifespan of the battery pack. The SoC change of each battery cell is shown in Figure 6.1.

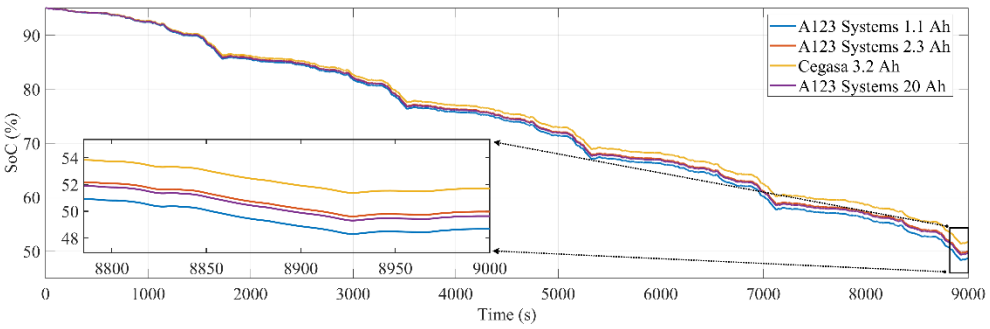

Figure 6.1 : State of charge change for each battery pack.

The designed battery packs with cells of different capacities and their total weights, along with the corresponding vehicle range values, are comparatively shown in Figure 6.2. In terms of total cell weight, the highest is the 1.1 Ah capacity battery from A123

Systems, while the lightest is their 20 Ah battery. The range values are inversely proportional to these weights, with the highest range achieved by the 20 Ah capacity battery, and the lowest range by the 1.1 Ah capacity battery.

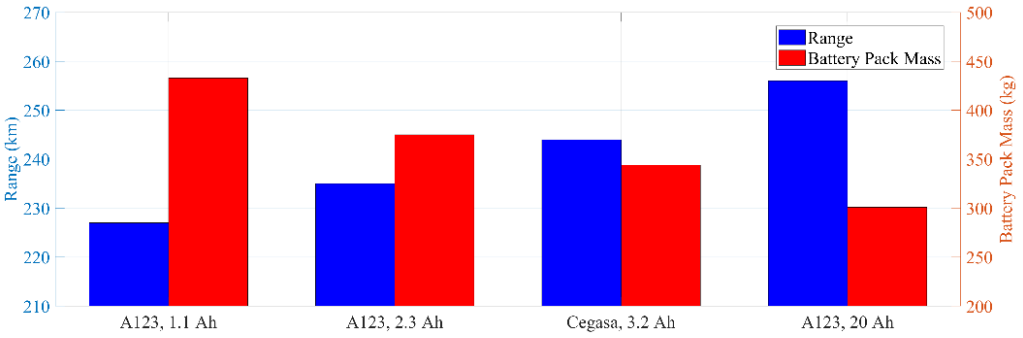

Figure 6.2 : EV battery pack mass vs range graph.

The design and chemical properties of battery cells exhibit different aging characteristics depending on environmental and usage conditions. Over a period of 10 years, with a 5 WLTP driving profile applied daily, the most significant aging was observed in the battery cell with a capacity of 3.2 Ah. In contrast, the least aging was seen in the battery cell with a capacity of 2.3 Ah. The battery aging results are shown in Figure 6.3.

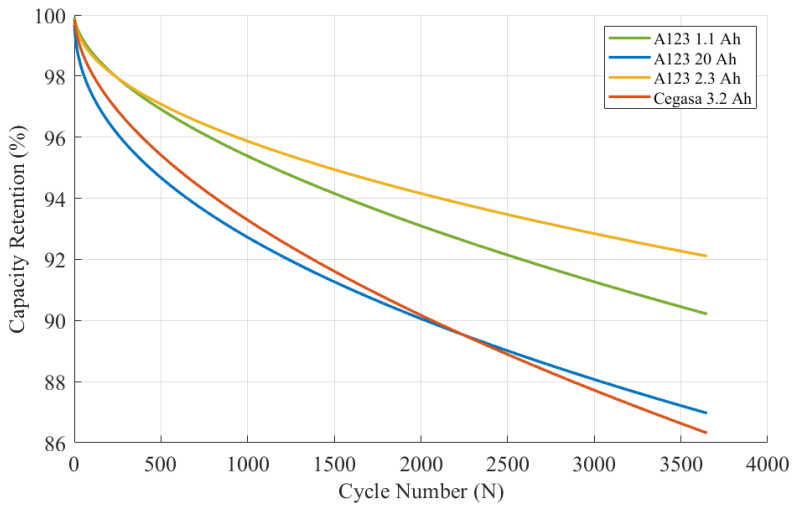

Figure 6.3 : Battery degradation graph of each battery pack.

The results obtained according to the cost function created in equation 4.5 are shown in Figure 6.4. Based on these results, the most suitable battery cell for the battery pack in terms of total volume, weight, price, and aging is determined to be the 2.3 Ah capacity battery from A123 Systems. It is planned to use this battery cell in the V2G application.

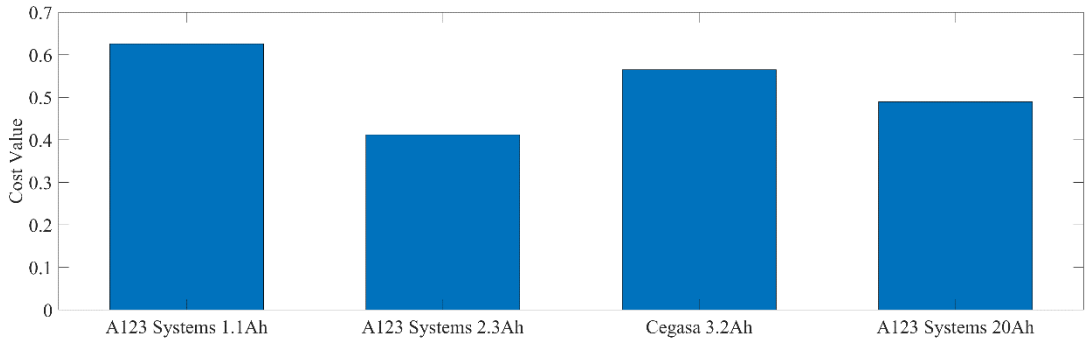

Figure 6.4 : Battery cells cost function values.

6.2 V2G Scheduling Optimization Results

Based on analyses conducted under various criteria, the battery lifespan was found to range between 7 and 14 years. This variability arises due to different usage scenarios and environmental conditions the battery is exposed to. More frequent and high-power V2G usage leads to faster battery aging, while less frequent and low-power usage extends the battery life. Figures 6.5 and 6.6 respectively show the battery aging graph obtained using 3.7 kW and 11 kW charging stations.

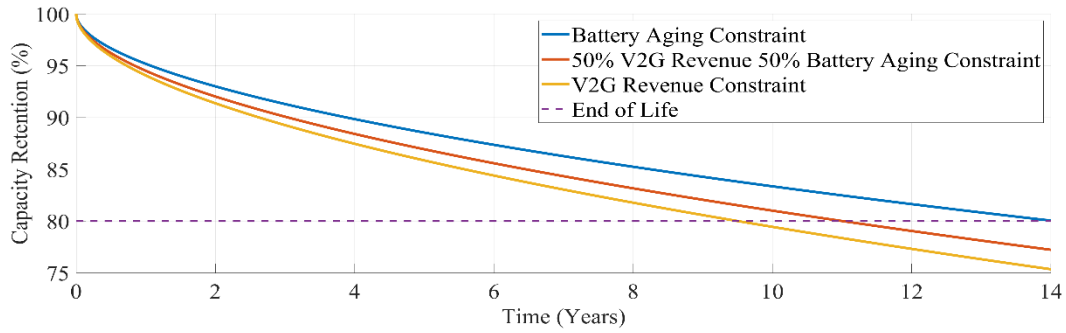

Figure 6.5 : Battery degradation with 3.7 kW charger.

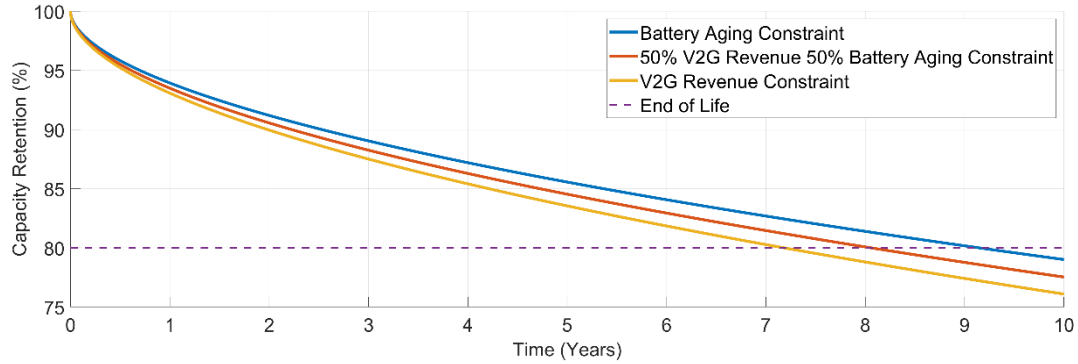

Figure 6.6 : Battery degradation with 11 kW charger.

In terms of V2G revenue, an annual range between €172 and €850 has been observed. This revenue range varies depending on the usable capacity of the battery, price fluctuations in the electricity market, and the frequency of services provided to the grid. Higher revenues are obtained with more frequent and high-power transfers, while lower revenues are associated with infrequent and low-power transfers. Figure 6.7 shows the revenues obtained for various V2G scenarios.

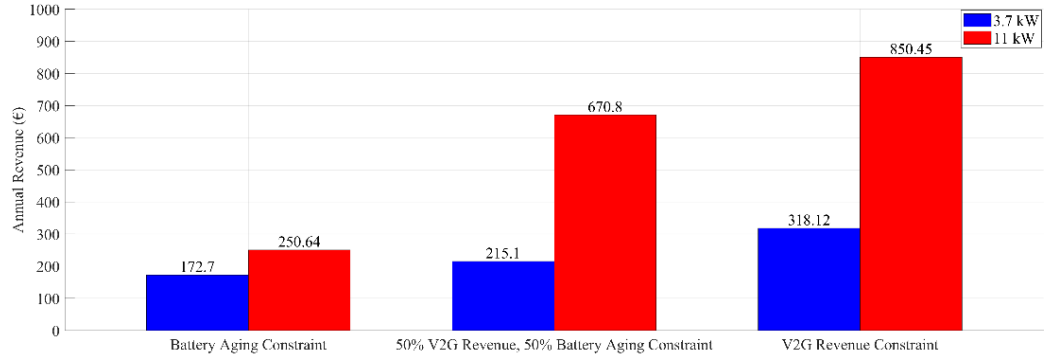

Figure 6.7 : V2G revenue comparison for each condition.

The results have revealed the effects of different power transfer levels on battery life and economic returns. It was determined that the battery life is the longest with a power transfer of 3.7 kW. This indicates that low-power transfers reduce stress and wear on the battery, thereby extending its life. Economically, it was found that an 11-kW power transfer provides the most favourable condition. This shows that high-power transfers generate higher revenues in shorter periods but shorten the battery's lifespan. Figure 6.8 presents a comparative analysis of V2G revenue and battery aging for each condition

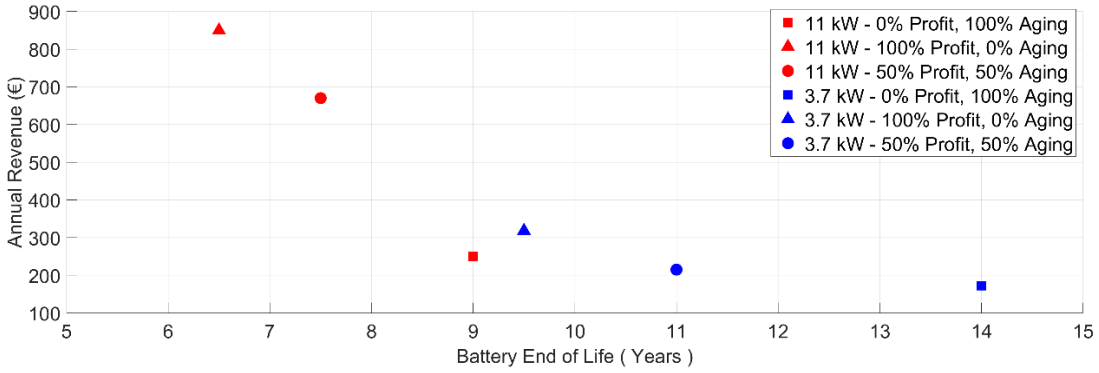

Figure 6.8 : Annual revenue vs battery life comparison of each condition.

7. CONCLUSION

This study examines frequency regulation services from the perspective of electric vehicle users. The objective is to evaluate the impact of vehicle-to-grid services on battery aging and economic returns. The process of connecting EVs to the grid for providing frequency regulation services was analyzed using a comprehensive model that considers various forces and factors. These include traction forces, road characteristics, environmental forces, auxiliary systems, driving profile, and gravitational forces. Battery aging mechanisms were evaluated using the Arrhenius model for lithium iron phosphate batteries, considering both cycle aging and calendar aging.A battery pack was designed using four different lithium iron phosphate battery cells, and a selection algorithm was developed. This process considered critical factors such as the volume, weight, cost, and aging of the battery pack. State of charge, state of health, and range data were analyzed for each battery cell to select the most suitable one.For planning V2G services, UK grid frequency data was used and clustered with the K-means classification algorithm. Daily frequency data was divided into thirty-minute periods, and optimization was performed using a binary genetic algorithm. As a scenario, the electric vehicle makes two trips every day. One trip occurs at 09:00 in the morning, and the other at 18:00 in the evening, each lasting thirty minutes. During each trip, the vehicle travels a total of twenty-three kilometers. The vehicle is charged every night between 23:00 and 23:59 and starts each day with an 80% state of charge. It is assumed that the vehicle is available to provide V2G frequency regulation services during the remaining time. The V2G service can operate bidirectionally when the state of charge is between 90% and 40%. If the state of charge is above 90%, the battery can only discharge through the V2G service. When the state of charge falls below 40%, the battery can only be charged through the V2G service. The optimization algorithm decides whether or not to provide vehicle-to-grid service during different periods of the day based on various weights. An optimal strategy is developed in accordance with grid demands and the vehicle owner's revenue expectations. Total of six different scenarios were examined. These scenarios involved evaluating the effects of different charging station powers, specifically 11 kW and 3.7 kW, on revenue and battery aging.

For each charging power, optimal results were obtained that minimize battery aging, maximize revenue, and balance 50% revenue with 50% battery aging. The impacts of power variations during EV charging and discharging processes on economic returns and battery life were discussed comparatively. It was observed that under various criteria, battery life ranged from 7 years to 14 years, while V2G revenue varied between €172 and €850 annually. The results showed that 11 kW charging stations provided higher income but also accelerated battery aging. In contrast, 3.7 kW charging stations resulted in lower income but also reduced battery aging. This was attributed to the higher stress on the battery from the higher charging power, which shortens battery life.Scenarios included evaluating the driving and charging behaviors of EVs, appropriate time periods for V2G services, and the effects of different charging station power levels.

REFERENCES

[1] **Tang, W., Zhu, Y., Hou, Y., Liu, L., Wu, Y., Loh, K. P., Zhang, H., & Zhu, K.** (2013). Aqueous rechargeable lithium batteries as an energy storage system of superfast charging. *Energy & Environmental Science*, 6(7), 2093. https://doi.org/10.1039/

[2] **E. Martinez-Laserna et al.** (2018). Technical Viability of Battery Second Life: A Study From the Ageing Perspective, *IEEE Transactions on Industry Applications*, vol. 54, no. 3, pp. 2703-2713, doi: 10.1109/TIA.2018.2801262

[3] **Ravi, S. S., & Aziz, M.** (2022). Utilization of Electric Vehicles for Vehicle-to-Grid Services: Progress and Perspectives. *Energies*, 15(2), 589. https://doi.org/10.3390/en15020589

[4] **M. Yilmaz and P. T. Krein.** (2012) Review of benefits and challenges of vehicle-to-grid technology, *IEEE Energy Conversion Congress and Exposition (ECCE)*, Raleigh, NC, USA, 2012, pp. 3082-3089, doi: 10.1109/ECCE.2012.6342356

[5] **Kester, J., Noel, L., De Rubens, G. Z., & Sovacool, B. K.** (2018). Promoting Vehicle to Grid (V2G) in the Nordic region: Expert advice on policy mechanisms for accelerated diffusion. *Energy Policy*, 116, 422–432. https://doi.org/10.1016/j.enpol.2018.02.024

[6] **Camargos, P. H., dos Santos, P. H., dos Santos, I. R., Ribeiro, G. S., & Caetano, R. E.** (2022). Perspectives on li-ion battery categories for Electric Vehicle Applications: A Review of State of the art. *International Journal of Energy Research*, 46(13), 19258–19268. https://doi.org/10.1002/er.7993

[7] **Preger, Y. et al.** (2020). Degradation of commercial lithium-ion cells as a function of chemistry and cycling conditions, *Journal of The Electrochemical Society*, 167(12), p. 120532. doi:10.1149/1945-7111/abae37

[8] **Wang S, Yu J.** (2021). A comparative life cycle assessment on lithium-ion battery: Case study on electric vehicle battery in China considering battery evolution. *Waste Management & Research*, 39(1), 156-164. doi:10.1177/0734242X20966637

[9] **Ding, Y., Cano, Z.P., Yu, A. et al.** (2019). Automotive Li-Ion Batteries: Current Status and Future Perspectives. *Electrochem. Energ*. Rev. 2, 1–28. https://doi.org/10.1007/s41918-018-0022-z

[10] **International Energy Agency.** (2022), Global Supply Chains of EV Batteries, IEA, Paris, https://www.iea.org/reports/global-supply-chains-of-ev-batteries

[11] **S. A. Amamra and J. Marco. (2019).** Vehicle-to-Grid Aggregator to Support Power Grid and Reduce Electric Vehicle Charging Cost, *IEEE Access*, vol. 7, pp. 178528-178538, doi: 10.1109/ACCESS.2019.2958664

[12] **Alfaverh, F., Denaï, M., & Sun, Y.** (2023). Optimal vehicle-to-grid control for supplementary frequency regulation using deep reinforcement learning. *Electric Power Systems Research*, 214, 108949. https://doi.org/10.1016/j.epsr.2022.108949

[13] **K. Ginigeme and Z. Wang.** (2020). Distributed Optimal Vehicle-To-Grid Approaches With Consideration of Battery Degradation Cost Under Real-Time Pricing, *IEEE Access*, vol. 8, pp. 5225-5235, doi: 10.1109/ACCESS.2019.2963

[14] **Miri, I., Fotouhi, A., Ewin, N.,** 2020. "Electric vehicle energy consumption modelling and estimation—a case study", International Journal of Energy Research, 45, 501-520.

[15] **Zhang, Y.T., Claudel, C.G., Hu, M.B., Yu, Y.H., Shi, C.L**., 2020. "Develop of a fuel consumption model for hybrid vehicles", *Energy Conversion and Management*, 207.

[16] **Wang, J., Besselink, I., & Nijmeijer, H.** (2017). Battery electric vehicle energy consumption prediction for a trip based on route information. Proceedings of the Institution of Mechanical Engineers, Part D: *Journal of Automobile Engineering*, 232(11), 1528–1542. https://doi.org/10.1177/0954407017729938.

[17] **Picard, A., Davis, R. S., Gläser, M., & Fujii, K.** (2008). Revised formula for the density of moist air (CIPM-2007). *Metrologia*, 45(2), 149–155. https://doi.org/10.1088/0026-1394/45/2/004.

[18] "The tyre," Société de Technologie Michelin, rue Breschet, 63000 Clermont-Ferrand, 2003. Accessed: May 27, 2023. [Online]. Available: http://docenti.ing.unipi.it/guiggianim/Michelin_Tire_Rolling_Resistance.pdf.

[19] **Kocaarslan, I., Zehir, M.A, Uzun, E., Uzun, E.C., Korkmaz, M.E., Cakiroglu, Y.** (2022). High-Fidelity Electric Vehicle Energy Consumption Modelling and Investigation of Factors in Driving on Energy Consumption, 4th Global Power, *Energy and Communication Conference*.

[20] **Gołębiewski, W., & Lisowski, M.** (2018). Theoretical analysis of electric vehicle energy consumption according to different driving cycles. *IOP Conference Series Materials Science and Engineering*, 421, 022010. https://doi.org/10.1088/1757-899x/421/2/022010

[21] **Url-1** <*https://dieselnet.com/standards/cycles/wltp.php/*>, date retrieved 15.07.2024.

[22] **Hughes, R., & Vagg, C.** (2022). Assessing the feasibility of a cold start procedure for solid state batteries in automotive applications. Batteries, 8(2), 13. https://doi.org/10.3390/batteries8020013

[23] **Lucaferri, V., Quercio, M., Laudani, A., & Fulginei, F. R.** (2023). A review on Battery Model-Based and Data-Driven Methods for battery

Management systems. *Energies*, 16(23), 7807. https://doi.org/10.3390/en16237807.

[24] **He, H., Xiong, R., & Fan, J.** (2011). Evaluation of Lithium-Ion battery equivalent circuit models for state of charge estimation by an experimental approach. *Energies*, 4(4), 582–598. https://doi.org/10.3390/en4040582.

[25] **Han, X., Lu, L., Zheng, Y., Feng, X., Li, Z., Li, J., & Ouyang, M**. (2019). A review on the key issues of the lithium ion battery degradation among the whole life cycle. *eTransportation*, 1, 100005. https://doi.org/10.1016/j.etran.2019.100005.

[26] **Tian, H., Qin, P., Li, K., & Zhao, Z**. (2020). A review of the state of health for lithium-ion batteries: Research status and suggestions. *Journal of Cleaner Production*, 261, 120813. https://doi.org/10.1016/j.jclepro.2020.120813.

[27] **Teodorescu, R., Sui, X., Vilsen, S. B., Bharadwaj, P., Kulkarni, A., & Stroe, D. I.** (2022). Smart Battery Technology for Lifetime Improvement. *Batteries*, 8(10), 169. https://doi.org/10.3390/batteries8100169.

[28] **Guo, Y., Cai, J., Liao, Y., Hu, J., & Zhou, X.** (2023). Insight into fast charging/discharging aging mechanism and degradation-safety analytics of 18650 lithium-ion batteries. *Journal of Energy Storage*, 72, 108331. https://doi.org/10.1016/j.est.2023.108331.

[29] **Woody, M., Arbabzadeh, M., Lewis, G. M., Keoleian, G. A., & Stefanopoulou, A**. (2020). Strategies to limit degradation and maximize Li-ion battery service lifetime - Critical review and guidance for stakeholders. *Journal of Energy Storage*, 28, 101231. https://doi.org/10.1016/j.est.2020.101231.

[30] **Collath, N., Tepe, B., Englberger, S., Jossen, A., & Hesse, H**. (2022). Aging aware operation of lithium-ion battery energy storage systems: A review. *Journal of Energy Storage*, 55, 105634. https://doi.org/10.1016/j.est.2022.105634.

[31] **Edge, J. S., O'Kane, S., Prosser, R., Kirkaldy, N. D., Patel, A. N., Hales, A., Ghosh, A., Ai, W., Chen, J., Yang, J., Li, S., Pang, M. C., Bravo Diaz, L., Tomaszewska, A., Marzook, M. W., Radhakrishnan, K. N., Wang, H., Patel, Y., Wu, B., & Offer, G. J.** (2021). Lithium ion battery degradation: what you need to know. Physical Chemistry Chemical Physics, 23(14), 8200–8221. https://doi.org/10.1039/d1cp00359c.

[32] **Xiong, R., Pan, Y., Shen, W., Li, H., & Sun, F.** (2020). Lithium-ion battery aging mechanisms and diagnosis method for automotive applications: Recent advances and perspectives. *Renewable and Sustainable Energy Reviews*, 131, 110048. https://doi.org/10.1016/j.rser.2020.110048.

[33] **Guo, J., Li, Y., Pedersen, K., & Stroe, D. I.** (2021). Lithium-Ion Battery Operation, Degradation, and Aging Mechanism in Electric Vehicles: An Overview. *Energies*, 14(17), 5220. https://doi.org/10.3390/en14175220.

[34] **Barré, A., Deguilhem, B., Grolleau, S., Gérard, M., Suard, F., & Riu, D**. (2013). A review on lithium-ion battery ageing mechanisms and estimations for automotive applications. *Journal of Power Sources*, 241, 680–689. https://doi.org/10.1016/j.jpowsour.2013.05.040.

[35] **Preger, Y., Barkholtz, H. M., Fresquez, A., Campbell, D. L., Juba, B. W., Romàn-Kustas, J., Ferreira, S. R., & Chalamala, B**. (2020). Degradation of commercial Lithium-Ion cells as a function of chemistry and cycling conditions. *Journal of the Electrochemical Society*, 167(12), 120532. https://doi.org/10.1149/1945-7111/abae37.

[36] **Vermeer, W., Mouli, G. R. C., & Bauer, P.** (2022). A comprehensive review on the characteristics and modeling of Lithium-Ion battery aging. *IEEE Transactions on Transportation Electrification*, 8(2), 2205–2232. https://doi.org/10.1109/tte.2021.3138357.

[37] **Wang, J., Liu, P., Hicks-Garner, J., Sherman, E., Soukiazian, S., Verbrugge, M., Tataria, H., Musser, J., & Finamore, P.** (2011). Cycle-life model for graphite-lifepo4 cells. *Journal of Power* Sources, 196(8), 3942–3948. https://doi.org/10.1016/j.jpowsour.2010.11.134.

[38] **J. Shen, S. Dusmez and A. Khaligh,** "Optimization of Sizing and Battery Cycle Life in Battery/Ultracapacitor Hybrid Energy Storage Systems for Electric Vehicle Applications," in *IEEE Transactions on Industrial Informatics*, vol. 10, no. 4, pp. 2112-2121, Nov. 2014, doi: 10.1109/TII.2014.2334233.

[39] **Martinez-Laserna, E., Sarasketa-Zabala, E., Sarria, I. V., Stroe, D., Swierczynski, M., Warnecke, A., Timmermans, J., Goutam, S., Omar, N., & Rodriguez, P.** (2018). Technical Viability of Battery Second Life: A Study from the Ageing Perspective. *IEEE Transactions on Industry Applications*, 54(3), 2703–2713. https://doi.org/10.1109/tia.2018.2801262.

[40] **Wang, J., Purewal, J., Liu, P., Hicks-Garner, J., Soukazian, S., Sherman, E., Sorenson, A., Vu, L., Tataria, H., & Verbrugge, M. W.** (2014). Degradation of lithium ion batteries employing graphite negatives and nickel–cobalt–manganese oxide + spinel manganese oxide positives: Part 1, aging mechanisms and life estimation. *Journal of Power Sources*, 269, 937–948. https://doi.org/10.1016/j.jpowsour.2014.07.030.

[41] A123 Systems, Inc. (2009). Technical datasheet of nanophosphate high power lithium ion cell APR 18650m1a battery.

[42] A123 Systems, Inc. (2006). Technical datasheet of nanophosphate high power lithium ion cell ANR 26650m1 battery.

[43] Cegasa Portable Energy, Technical datasheet of lithium ion cell LFP 3.2 26650 battery.

[44] A123 Systems, Inc. (2011). Technical datasheet of nanophosphate lithium ion prismatic pouch cell AMP20m1hd-a battery.

[45] **Iacobucci, R., McLellan, B., & Tezuka, T.** (2018). Modeling shared autonomous electric vehicles: Potential for transport and power grid

integration. *Energy*, 158, 148–163. https://doi.org/10.1016/j.energy.2018.06.024.

[46] **Amamra, S. A., & Marco, J.** (2019). Vehicle-to-Grid Aggregator to support power grid and reduce electric vehicle charging cost. IEEE Access, 7, 178528–178538. https://doi.org/10.1109/access.2019.2958664.

[47] **Staudt, P., Schmidt, M., Gärttner, J., & Weinhardt, C.** (2018). A decentralized approach towards resolving transmission grid congestion in Germany using vehicle-to-grid technology. *Applied Energy*, 230, 1435–1446. https://doi.org/10.1016/j.apenergy.2018.09.045.

[48] **Fan, H., Jiang, L., Zhang, C. K., & Mao, C**. (2016). Frequency regulation of multi-area power systems with plug-in electric vehicles considering communication delays. *IET Generation, Transmission & Distribution*, 10(14), 3481-3491.

[49] **Huda, M., Koji, T., & Aziz, M.** (2020). Techno Economic Analysis of Vehicle to Grid (V2G) Integration as Distributed Energy Resources in Indonesia Power System. *Energies*, 13(5), 1162. https://doi.org/10.3390/en13051162.

[50] **Fitzgerald, G., Garrett, J., Mandel, J., Morris, J., & Touati, H.** (2015). The Economics of Battery Energy Storage: How multi-use, customer-sited batteries deliver the most services and value to customers and the grid. Rocky Mountain Institute.

[51] **Tan, K. M., Ramachandaramurthy, V. K., & Yong, J. Y.** (2016). Integration of electric vehicles in smart grid: a review on vehicle to grid technologies and optimization techniques. Renewable and Sustainable *Energy Reviews*, 53, 720-732.

[52] IEA (2022), Global Supply Chains of EV Batteries, IEA, Paris https://www.iea.org/reports/global-supply-chains-of-ev-batteries.

[53] **Thingvad, A., Calearo, L., Andersen, P. B., Marinelli, M., Neaimeh, M., Suzuki, K., & Murai, K.** (2019). Value of V2G frequency regulation in Great Britain considering real driving data. *IEEE PES Innovative Smart Grid Technologies Europe*. https://doi.org/10.1109/isgteurope.2019.8905679

CURRICULUM VITAE

Name Surname : Arda AKYILDIZ

EDUCATION:

- **B.Sc.:** 2022, Istanbul Technical University, Faculty of Electrical and Electronics Engineering, Electrical Engineering Department

PUBLICATIONS, PRESENTATIONS AND PATENTS ON THE THESIS:

- **Akyildiz A.,** Ergun B. E., Zehir M. A., Gulbahce M. O., (2024). V2G Approaches Considering Battery Health for Electric Vehicles. *3rd International Graduate Research Symposium (IGRS).*

OTHER PUBLICATIONS, PRESENTATIONS AND PATENTS:

- Ciftci D., **Akyildiz A**., Ergun B.E., Gulbahce M. O. (2023). An Analytical Comparison of Interleaved Boost Converters with Different Inductor Configurations. *Turkish Journal of Electrical Power and Energy Systems.*
- Hakki Y., **Akyildiz A**., Gulbahce M. O., (2024). A Comprehensive Review of Physics-Based Battery Models and Comparing Different Physics Based Models for Various. *Turkish Journal of Electrical Power and Energy Systems.*
- Aydin O.S., Lordoglu A., Lordoglu M., **Akyildiz A**., Ergun B.E. and Gulbahce M.O., (2024). Meta-Heuristics Based Design and Optimization of Active Clamp Flyback Converter for USB PD. *IEEE Access*, doi: 10.1109/ACCESS.2024.3368861
- Ciftci D., **Akyildiz A**., Ergun B.E., Gulbahce M. O. (2023). A Comparative Study for Interleaved Boost Converter with coupled/Uncoupled Inductors. *ELECO 2023 International Conference on Electrical and Electronics Engineering*.